Weather and Climate Extremes 34 (2021) 100391

Contents lists available at ScienceDirect

Weather and Climate Extremes

journal homepage: www.elsevier.com/locate/wace

Future intensification of precipitation and wind gust associated thunderstorms over Lake Victoria

Jonas Van de Walle [a,*], Wim Thiery [b], Roman Brogli [c], Olivia Martius [d,e], Jakob Zscheischler [e,f,g], Nicole P.M. van Lipzig [a]

[a] Department of Earth and Environmental Sciences, KU Leuven, Leuven, Belgium
[b] Department of Hydrology and Hydraulic Engineering, Vrije Universiteit Brussel, Brussels, Belgium
[c] Institute for Atmospheric and Climate Science, ETH Zurich, Zürich, Switzerland
[d] Institute of Geography, University of Bern, Bern, Switzerland
[e] Oeschger Centre for Climate Change Research, University of Bern, Bern, Switzerland
[f] Department of Computational Hydrosystems, Helmholtz Centre for Environmental Research – UFZ, Leipzig, Germany
[g] Climate and Environmental Physics, University of Bern, Bern, Switzerland

ARTICLE INFO

Keywords:
Lake Victoria
Regional climate modeling
Climate projections
Severe wind gusts
Intense precipitation
Compound events

ABSTRACT

Severe thunderstorms affect more than 30 million people living along the shores of Lake Victoria (East Africa). Thousands of fishers lose their lives on the lake every year. While deadly waves are assumed to be initiated by severe wind gusts, knowledge about thunderstorms is restricted to precipitation or environmental proxies. Here we use a regional climate model run at convection-permitting resolution to simulate both precipitation and wind gusts over Lake Victoria for a historical 10-year period. In addition, a pseudo global warming simulation provides insight into the region's future climate. In this simulation, ERA5's initial and boundary conditions are perturbed with atmospheric changes between 1995–2025 and 2070–2100, projected by CMIP6's ensemble mean. It was found that future decreases in both mean precipitation and wind gusts over Lake Victoria can be attributed to a weaker mean mesoscale circulation that reduces the trigger for over-lake nighttime convection and decreases the mean wind shear. However, an intensification of extremes is projected for both over-lake precipitation and wind gusts. The observed ~7 $\%K^{-1}$ Clausius–Clapeyron extreme precipitation scaling is ascribed to increased water vapor content and a compensation of weaker mesoscale circulations and stronger thunderstorm dynamics. More frequent wind gust extremes result from higher wind shear conditions and more compound thunderstorms with both intense rainfall and severe wind gusts. Overall, our study emphasizes Lake Victoria's modulating role in determining regional current and future extremes, in addition to changes expected from the Clausius–Clapeyron relation.

1. Introduction

As one of world's stormiest places on Earth, Lake Victoria claims the lives of thousands of fishers each year (Semazzi, 2011; Cannon et al., 2014). Capsizing accidents with passenger ferries and transport boats are frequently reported and survivors from such accidents tell about strong waves hitting the vessel, shattering it into pieces (Kiwanuka-Tondo et al., 2019). Many studies over Lake Victoria assume that such waves are directly related to severe thunderstorms and aim at better understanding the climatic conditions leading to precipitation extremes in the Lake Victoria basin (Chamberlain et al., 2014; Thiery et al., 2016; Woodhams et al., 2019; Finney et al., 2020). Worldwide, convective precipitation is strongly influenced by frontal systems, orography or local temperature fluctuations and gradients (Torma et al., 2015; Giorgi et al., 2016; Schemm et al., 2016; Helsen et al., 2020). Over Lake Victoria in particular, the lake-land temperature contrast results in region-specific mesoscale circulations, which are of major importance to thunderstorm initiation (Anyah et al., 2006; Thiery et al., 2015; Woodhams et al., 2019; Van de Walle et al., 2020). A faster warming land than lake initiates afternoon lake breezes and associated over-lake subsidence, suppressing convection. Nighttime land breezes however, resulting from a positive lake-land temperature contrast, converge over the lake and often form the necessary trigger for thunderstorm development. This trigger mechanism is projected to reduce in a warmer climate, causing lower total over-lake rainfall (Thiery et al., 2016).

* Correspondence to: Celestijnenlaan 200e, Leuven, Belgium.
E-mail address: jonas.vandewalle@kuleuven.be (J. Van de Walle).

https://doi.org/10.1016/j.wace.2021.100391
Received 12 April 2021; Received in revised form 22 September 2021; Accepted 19 October 2021
Available online 28 October 2021

Despite this overall precipitation decrease, future projections over Lake Victoria unanimously conclude an intensification of extreme over-lake rainfall (Thiery et al., 2016; Kendon et al., 2019; Finney et al., 2020). Such rainfall intensification with climate change is extensively studied for regions worldwide and theoretically described by the Clausius–Clapeyron relation, which is based on the higher moisture-holding capacity of a warmer atmosphere, potentially providing more moisture to rainfall events (Westra et al., 2014). While mean global precipitation increases with 1–3%K^{-1} (Allen and Ingram, 2002; Held and Soden, 2006), sub-daily convective rainfall extremes increase at a rate of about 6%–7% per degree warming (Ban et al., 2015) or regionally even higher (Fowler et al., 2021). Though this scaling has been confirmed over many regions worldwide (Trenberth et al., 2003; Hardwick Jones et al., 2010; O'Gorman and Muller, 2010; Trenberth, 2011; Kharin et al., 2013; Chan et al., 2016), in tropical regions it is highly variable across different models (Kharin et al., 2007; Allan and Soden, 2008; O'Gorman, 2012, 2015; Taylor et al., 2017).

This variability can generally be related to different factors which may cause extreme precipitation changes to deviate regionally from Clausius–Clapeyron scaling. First, large-scale atmospheric circulation changes can affect total precipitation and rainfall extremes (Otto et al., 2016; Fowler et al., 2021). In the Lake Victoria region in particular, blocking effects of easterly trade winds by high mountains were already shown to influence the rainfall location and over-lake intensity (Van de Walle et al., 2020). Second, updraft velocity changes within thunderstorms can also play a role in explaining deviations from Clausius–Clapeyron (Emori and Brown, 2005; Muller et al., 2011; Berg et al., 2013). Using convective available potential energy (CAPE) as a proxy for the maximal strength of the convective updraft, Earth system models unanimously project higher CAPE with warming climate (Sobel and Camargo, 2011; Brooks, 2013; Singh et al., 2017), as confirmed by regional convection-permitting models (Romps, 2011; Rasmussen et al., 2020) and supported by theoretical considerations (Del Genio et al., 2007; Seeley and Romps, 2015b; Romps, 2016). Third, a reduced triggering mechanism might decrease the number of initiated thunderstorms (Thiery et al., 2016). Fourth, additional deviations from Clausius–Clapeyron are possible when organization of convection changes (Singleton and Toumi, 2013; Fowler et al., 2021).

Besides intense precipitation, thunderstorms can also be accompanied by strong winds. From an impact point of view, their association to sharp, high and deadly waves makes them particularly important in the Lake Victoria region. Concretely, wind is shown to determine wave growth, and wind gusts can have a big impact on the shape and magnitude of (lake) waves (Abdalla and Cavaleri, 2002; Cavaleri et al., 2007; Šepić and Rabinovich, 2014; Li et al., 2018). However, information about wind gust strengths or future projections are missing for the Lake Victoria region. Yet, some studies describe the atmospheric conditions fueling wind gusts, applied to different regions worldwide (Brooks et al., 2003; Trapp et al., 2007; Muller, 2013; Taylor et al., 2017; Púčik et al., 2017). These conditions include CAPE and vertical wind shear over a deep atmospheric layer (surface-6 km, Brooks et al., 2003 or surface-500 hPa, Púčik et al., 2017). Wind shear is assumed to (i) organize thunderstorms that often accompany severe wind gusts (Weisman and Klemp, 1982; Doswell, 2001; Trapp et al., 2007; Markowski and Richardson, 2011; Muller, 2013; Taylor et al., 2017), (ii) prolong storms by physically displacing deep-convective updrafts from rain shafts (Seeley and Romps, 2015a) and (iii) promote storm-scale rotation and tornadoes (Trapp and Hoogewind, 2016). In addition, CAPE represents vertical movement which helps rear-inflow jets to transport strong horizontal momentum down toward the surface (Markowski and Richardson, 2011). Not included by studying those atmospheric environments, are non-rotating winds from unstructured convective storms, which are almost always associated with the precipitation-cooled outflow, via evaporation, melting or sublimation (Markowski and Richardson, 2011; Zinner and Groenemeijer, 2012).

However, a first important caveat is that favorable environments are not the same as storms occurrence (Sobel and Tippett, 2018). For example, Trapp and Hoogewind (2016) suggest that increases in actual storm frequency and intensity in a warmer climate might be less pronounced than expected from changes in the environmental proxies. Therefore, this study avoids the dependency on environmental proxies by analyzing both intense precipitation and severe wind gust changes over Lake Victoria directly from present-day and future convection-permitting multi-year climate simulations. Such convection-permitting climate simulations form a reliable tool for this study, as their representation of extreme precipitation is largely improved compared to coarser-resolution simulations (Prein et al., 2015; Brisson et al., 2016; Vanden Broucke et al., 2019; Kendon et al., 2019; Finney et al., 2019; Coppola et al., 2020).

Future projections are obtained by applying a 'pseudo global warming' approach (Schär et al., 1996; Kawase et al., 2009; Rasmussen et al., 2011; Kröner et al., 2017; Liu et al., 2017; Prein et al., 2017b; Brogli et al., 2019; Hentgen et al., 2019; Rasmussen et al., 2020), conferring three major advantages over the traditional downscaling. First, the use of an ensemble mean climate change signal is more robust than the signal from individual members. If most members agree, their common signal is also given by the ensemble mean. Otherwise the signal is small, which reflects the uncertainty. Second, the use of 30-year averaged fields eliminates natural decadal variability, thus better reflecting the anthropogenically forced climate change signal. Consequently, the simulation periods can be reduced to 10 year, instead of typically 30 year for traditional downscaling approaches (Yoshikane et al., 2013), making the pseudo global warming approach especially attractive for computationally expensive and storage demanding high resolution simulations. Third, the high resolution of the (perturbed) ERA5 dataset allows direct downscaling to convection-permitting scales without intermediate nesting steps.

A second caveat is that hazard studies over Lake Victoria focus on precipitation, while wind and wind gusts might be more relevant from an impact point of view. Therefore, this study treats over-lake intense precipitation and severe wind gusts as compound events (Zscheischler et al., 2018, 2020). As a result, this study looks at precipitation only, wind gust only and compound events with intense precipitation and severe wind gusts occurring together.

2. Methods

2.1. Regional climate model

Climate simulations are performed with the three-dimensional non-hydrostatic regional climate model COSMO-CLM version 5.0 (Rockel et al., 2008). In our setup the following components and processes are parameterized: radiative transfer (Ritter and Geleyn, 1991), turbulence (Mironov and Raschendorfer, 2001), shallow convection (Tiedtke, 1989), land surface (TERRA-ML, Grasselt et al., 2008; Schulz et al., 2015; Mironov et al., 2010), lake (FLake, Mironov et al., 2010), clouds and microphysics (two-moment scheme, Seifert and Beheng, 2001, 2006).

The evaluated model configuration is identical to Van de Walle et al. (2020) and originates from the COSMO-CLM contribution to the CO-ordinated Regional Climate Downscaling EXperiment simulations over Africa (CORDEX-Africa, Giorgi et al., 2009; Nikulin et al., 2012; Dosio and Panitz, 2016). The configuration contains 70 vertical layers up to 30 km model height, allowing for deep tropical convection. In contrast to previous COSMO-CLM set-ups for the region (Akkermans et al., 2014; Thiery et al., 2015, 2016), deep convection is explicitly permitted thanks to the high horizontal resolution of 0.025° (~2.8 km). The domain spans 5.0°S–2.5°N, 27.5°–38.5°E, covering the Lake Victoria basin as well as the surrounding western and eastern mountain ranges (Fig. 1). Though precipitation has been evaluated in Van de Walle

Table 1
List of CMIP6 models combined to produce perturbation fields applied by the pseudo global warming approach. At the moment of downloading, these models had necessary fields available on multiple pressure levels.

No.	CMIP6 model name	Country	Hor. res. (lon. by lat.)	Variant label	Key reference
1	BCC-CSM2-MR	China	1.1° × 1.1°	r1i1p1f1	Wu et al. (2019)
2	CanESM5	Canada	2.8° × 2.8°	r1i1p1f1	Swart et al. (2019)
3	CESM2	USA	1.3° × 0.9°	r1i1p1f1	Lauritzen et al. (2018)
4	CESM2-WACCM	USA	1.3° × 0.9°	r1i1p1f1	Li (2019)
5	CNRM-CM6–1	France	1.4° × 1.4°	r1i1p1f2	Voldoire et al. (2019)
6	CNRM-ESM2–1	France	1.4° × 1.4°	r1i1p1f2	Séférian et al. (2019)
7	EC-Earth3	Europe	0.7° × 0.7°	r1i1p1f1	Massonnet et al. (2020)
8	EC-Earth3-Veg	Europe	0.7° × 0.7°	r1i1p1f1	Not available
9	FGOALS-g3	China	2.0° × 2.3°	r3i1p1f1	He et al. (2019)
10	GFDL-ESM4	USA	1.3° × 1.0°	r1i1p1f1	Held et al. (2019)
11	INM-CM4–8	Russia	2.0° × 1.5°	r1i1p1f1	Volodin et al. (2018)
12	INM-CM5–0	Russia	2.0° × 1.5°	r1i1p1f1	Volodin et al. (2018)
13	IPSL-CM6A-LR	France	2.5° × 1.3°	r1i1p1f1	Not available
14	MIROC6	Japan	1.4° × 1.4°	r1i1p1f1	Tatebe et al. (2019)
15	MPI-ESM1-2-HR	Germany	0.9° × 0.9°	r1i1p1f1	Gutjahr et al. (2019)
16	MRI-ESM2–0	Japan	1.1° × 1.1°	r1i1p1f1	Yukimoto et al. (2019)
17	NESM3	China	1.9° × 1.9°	r1i1p1f1	Cao et al. (2018)
18	UKESM1-0-LL	UK	1.9° × 1.3°	r1i1p1f1	Sellar et al. (2019)

et al. (2020), an additional evaluation against some in-situ observations is provided in the supplementary material. Evaluating compound precipitation-wind extremes is more challenging but it can be expected that high-resolution simulations are much more realistic than reanalysis data, in particular over complex topography (Zscheischler et al., 2021).

For the present-day (PD, 2005–2016) simulations, the direct lateral forcing is provided by the recent high-resolution (~31 km) European Centre for Medium-Range Weather Forecasts fifth reanalysis product (ERA5, Hersbach et al., 2020). The end-of-century (EoC, 2080–2091) COSMO-CLM climate projections are forced by ERA5 plus a climate signal perturbation from the Coupled Model Intercomparison Project Phase 6 (CMIP6, Eyring et al., 2016, 2019; Almazroui et al., 2020) ensemble, applying a 'pseudo global warming' approach.

2.2. Pseudo global warming projections

Many studies have applied such 'pseudo global warming' approach (Schär et al., 1996; Kawase et al., 2009; Rasmussen et al., 2011; Kröner et al., 2017; Liu et al., 2017; Prein et al., 2017b; Brogli et al., 2019; Hentgen et al., 2019; Rasmussen et al., 2020), either considering one Earth system model, or an ensemble mean from CMIP3 or CMIP5. We follow the procedure described by Kröner et al. (2017) and Brogli et al. (2019) to create perturbation fields for temperature, specific humidity and horizontal wind from the CMIP6 ensemble members listed in Table 1, containing the complete list for which pressure level information was available at the Earth System Grid Federation (ESGF) nodes. If available, (near-)surface variables (surface pressure, two-meter temperature, two-meter specific humidity and ten-meter meridional and zonal wind), as well as temperature, specific humidity and both wind components at the 1000, 850, 700, 500, 250, 100, 50 and 10 hPa pressure levels are downloaded for each model, following the high-emission shared socioeconomic pathway (SSP5-8.5). The 30-year periods 1995–2025 and 2070–2100 are chosen, perfectly covering the 10-year COSMO-CLM simulation periods.

The resulting CMIP6 data is then processed systematically to produce perturbations for each variable that temporally and spatially match ERA5. First, multi-year averages for each variable are computed, resulting in an annual cycle with daily temporal resolution for each CMIP6 member. Second, all fields are bilinearly (for temperature and wind components) or second order conservatively (for specific humidity) remapped to the ERA5 grid. Third, the ensemble mean per variable is computed, delivering a good approximation for the climatology at a present-day period (averaging 1995–2025) and end-of-century period (averaging 2070–2100). Fourth, a global CMIP6 ensemble-mean climate change signal under the high-emission scenario SSP5-8.5 is computed as the difference:

$$\Delta X_{\mathrm{CMIP6}} = X^{\mathrm{EoC}}_{\mathrm{CMIP6}} - X^{\mathrm{PD}}_{\mathrm{CMIP6}}, \tag{1}$$

for each variable X. Fifth, to avoid unrealistic day-to-day variations, the difference fields are temporally smoothed by keeping only the three main Fourier components of the annual cycle (Bosshard et al., 2011; Brogli et al., 2019). Sixth, a spatial Gaussian filter removes strong pixel-to-pixel deviations, after which a linear vertical interpolation from all pressure and surface layers to the ERA5 model levels is performed. Last, another linear interpolation translates the daily to hourly difference fields. As a result, the initial and boundary conditions driving the end-of-century convection-permitting projection are produced for each variable X by:

$$X^{\mathrm{perturbed}}_{\mathrm{ERA5}} = X_{\mathrm{ERA5}} + \Delta X_{\mathrm{CMIP6}}. \tag{2}$$

2.3. Extreme value analysis

To answer the question whether Lake Victoria's most extreme precipitation and wind gust events will intensify in a warmer climate, all hourly over-lake events are pooled and values exceeding a high threshold are fitted to a General Pareto Distribution (GPD, Coles et al., 2001):

$$G_{\xi,\beta}(x) = 1 - \left(1 + \frac{\xi x}{\beta}\right)^{-1/\xi}, \tag{3}$$

with x the excess over a chosen threshold value u. The distribution is defined by the shape and scale parameters, respectively ξ and β, which are estimated using the maximum-likelihood method. Subtle, but crucial for a proper fitting, is the threshold definition above which an event is considered as extreme. Following Coles et al. (2001), this threshold is chosen based on the parameter stability plots, visualizing the variation in the estimated parameters $\hat{\xi}$ and $\hat{\beta}$ while manually increasing the threshold value u. Little variation with increasing u implies a stable and reliable fit. The fitting and threshold choosing, as well as creating return level plots are done using the recent Python package *thresholdmodeling* (Lemos et al., 2020), embedding the *extRemes* R package (Gilleland and Katz, 2016).

2.4. Definition of event, event-peak and event-peak preceding condition

A single 'precipitation event' is defined per grid box by rainfall intensities consecutively exceeding the 1 mm/h threshold. Similarly, a 'wind gust event' is defined by the period during which the hourly

maximal wind gust is above 15 m/s. Importantly, because the focus is on extremes well above this threshold, the exact choice does not largely affect the results (not shown). Events are defined per grid box, though in reality, thunderstorms possibly cover multiple grid boxes. In addition, each event is characterized by an 'event-peak', the maximal rainfall or wind gust during the event. Most analyses select the most extreme event-peaks, referred to with their respective present-day over-lake percentile, computed directly from all possible conditions that also include dry or windstill situations. For example, the 99.99th present-day over-lake percentile corresponds to 50.5 mm/h rainfall or 24.2 m/s wind gust, while the 99.999th percentile corresponds to 72.9 mm/h rainfall or 27.8 m/s wind gust. Over the full 10-year period, approximately 100 000 h exceed the 99.99th percentile somewhere over the lake, only 10 000 exceed the 99.999th percentile. On average, this corresponds to respectively 8.8 and 0.88 h per lake pixel.

Statistical significance is tested on both mean and extreme precipitation and wind gusts. Each year of the 10-year simulation period is considered separately, and the ten resulting values together form a distribution. Both present-day and end-of-century distributions are statistically compared with a t-test and conclusions are made at 5% significance level.

Supplementary to 'precipitation only' or 'wind gust only' events, compound events correspond to thunderstorms producing both intense precipitation and severe wind gusts. They are retrieved in three steps. First, for each precipitation event-peak, the most severe wind gust is selected within a radius of 5 pixels (~14 km) and an enclosing time period of 5 h (−2 h to +2 h, both inclusive). Second, for each wind gust event-peak, the most intense precipitation is searched in the same way. Third, double counted events during the previous steps are removed. The timing of the compound event-peak is inherited from the earliest precipitation or wind gust event-peak.

We subsequently consider four atmospheric variables which are maximized over 3 h preceding the precipitation, wind gust or compound event-peak (−2 h to 0 h). First, over-lake mass flux convergence at 850 hPa provides insight into the mesoscale circulation pattern and associated thunderstorm trigger possibility. The quantity is defined as:

$$lake MFC850 = -\iint_{LV} \left(\vec{\nabla} \cdot \rho\vec{v}\right) dA, \tag{4}$$

with ρ the air density and $\vec{v}$ the horizontal wind, both at 850 hPa. Second, the maximal vertical updraft velocity ($VWmax$) is maximized over time, over the 70 available vertical model layers as well as over a radius of 5 pixels around the rainfall or wind gust event-peak. This spatial maximization over neighboring pixels allows a physical displacement of updraft and rain shaft, while the 3 h maximization allows for temporal lag between the updraft and the precipitation or wind gust. Third, maximal wind shear ($S06max$) quantifies the maximal horizontal wind vector difference between different vertical layers below 6 km height, averaged over a radius of 5 pixels around the rainfall or wind gust event-peak. This spatial averaging avoids the wind shear to be influenced by the low-level wind gusts. Fourth, total column-integrated water vapor (TQV) is retrieved to investigate the importance of available water to produce extreme thunderstorms. Following the well-studied Clausius–Clapeyron relation, this is the major and most obvious driver for future precipitation changes.

3. Results

3.1. Thunderstorm changes

Based on global precipitation projections, an annual mean increase in precipitation by 1–2%K^{-1} is expected (Allen and Ingram, 2002; Held and Soden, 2006; Westra et al., 2014). Accordingly, our high-resolution simulations project more rainfall over land. However, the annual mean precipitation over Lake Victoria surprisingly decreases (Fig. 1a–c). Yet this decrease does not remove the lake's outstanding rainfall maximum in the region, along with the rainfall maximums over the dense rainforest in the west and some mountain peaks that trigger orographic convection. In contrast to this reduced mean over-lake precipitation towards the end of the century, intense thunderstorms occur more often (Fig. 1d–f), with 'intense' defined as rainfall event-peaks exceeding 50.5 mm/h, that is, the 99.99th present-day percentile. This intense rainfall increase is systematic over the entire Lake Victoria area, ranging from 0 to over 50%. Detailed insight into the intense precipitation increase is gained by summarizing all most intense over-lake rainfall event-peaks in a return level plot (Fig. 2a), visualizing the occurrence frequency of a certain event-peak somewhere over the lake. The figure includes both present-day and end-of-century modeled high-intensity event-peaks, as well as their corresponding Generalized Pareto fits. The statistical significant climate change signal from present-day to end-of-century can be interpreted in two ways. First, high-intensity event-peaks occur more often in future. For example, the frequency of a 150 mm/h event-peak increases from once every 10 years under present-day climate to more than once per year by the end of the century. Second, low-frequency event-peaks become more intense. For example, a once-in-a-year hourly event-peak produces ~135 mm rain under current climate conditions, while its intensity is projected to increase up to ~155 mm.

This modeled frequency/intensity increase of extreme over-lake precipitation event-peaks is compared against the return levels expected from pure Clausius–Clapeyron considerations: 7%K^{-1} with an over-lake mean near-surface temperature increase of 2.4 K, computed as the mean difference between the end-of-century and present-day simulations as described in Section 3.3. Both theoretical and modeled future precipitation intensifications are remarkably consistent, at first sight suggesting pure thermodynamic effects. However, as argued later, a weakened triggering mechanism for thunderstorm initiation is compensated by individual thunderstorm intensification via strengthened updrafts, ultimately resulting in a Clausius–Clapeyron-like future scaling.

Mean hourly wind gust strength is generally projected to decrease almost over the entire domain (Fig. 1g–i). Largest changes are observed over Lake Victoria and near the eastern mountains. In contrast to the mean wind gusts, the trend of severe wind gusts exceeding the 99.99th present-day percentile, is less clear (Fig. 1j–l). However, pooling all over-lake event-peaks and zooming to the most severe ones, reveal a clear shift to more severe wind gusts (Fig. 2b). A present-day once-in-a-year wind gust event-peak of ~36 m/s intensifies to ~40 m/s in the end-of-century simulation. Remarkably, this shift is only seen for the most severe event-peaks with wind speeds exceeding ~30 m/s, which also explains why Fig. 1l did not show this clear signal. This shift is statistically significant, except for very high return periods, where the statistical t-test could not exclude this climate change signal to be purely due to the high uncertainties.

3.2. Compound intense precipitation and severe wind gust events

Besides occasional hailstones or damaging tornadoes, thunderstorms are most often accompanied by intense rainfall, severe wind gusts or a combination of the two. A dependence analysis provides particular insight into the relevance and occurrence of the combined class, called compound events (Fig. 3). The relative frequency distribution of maximal wind gust in a five hour time window around the considered rainfall event-peaks is shown for different precipitation intensity bins (Fig. 3a). For each bin, the distribution peaks at ~13 m/s. The chance of exceeding 20.2 m/s, the threshold which one million event-peaks exceed, is visualized in Fig. 3b. The chance of strong wind gusts, given a rainfall event-peak that exceeds 10 mm/h, varies between ~7 and 16%, with the highest chances corresponding to the most intense rainfall event-peaks. These low chances suggest that many simulated thunderstorms over Lake Victoria are intense 'precipitation only' events, accompanied by weak to moderate wind gusts.

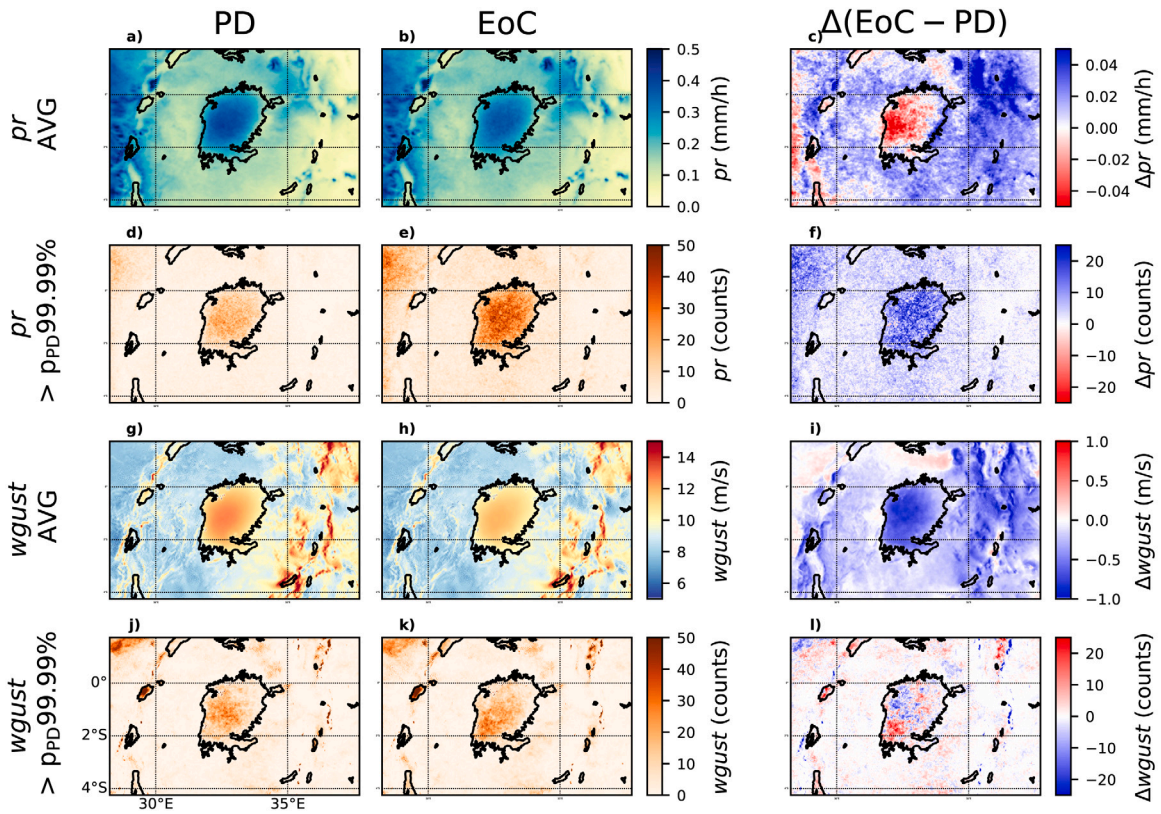

Fig. 1. Present-day (PD) and end-of-century (EoC) hourly rainfall (pr) and maximal hourly wind gust (wgust) averages, as well as their absolute frequencies exceeding the 99.99th present-day percentile, thus showing about 100 000 over-lake event-peaks. Absolute differences are included in the right column. Data is produced by two 10-year COSMO-CLM simulations, covering the periods 2006–2015 and 2081–2090, the latter applying the pseudo global warming approach.

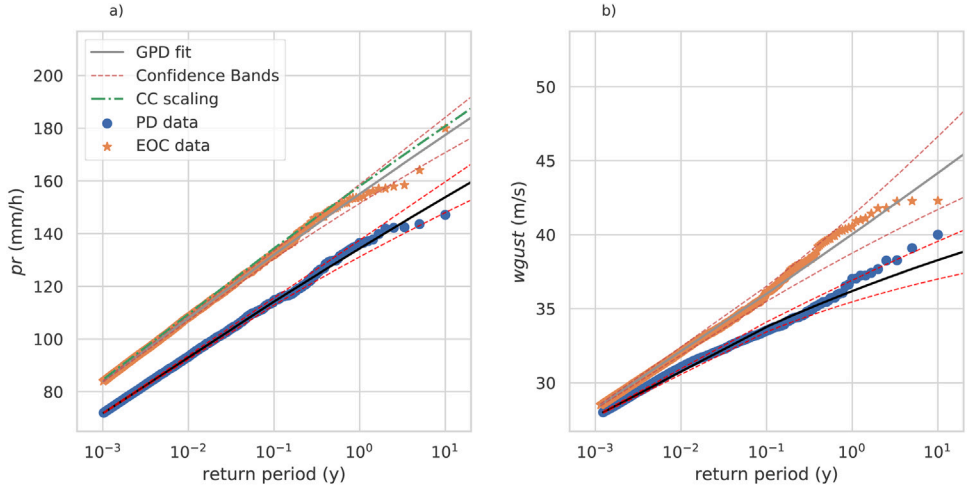

Fig. 2. Present-day (PD, blue dots) and end-of-century (EoC, orange stars) hourly rainfall and maximal hourly wind gust return periods of all over-lake simulation data exceeding the 99.999th percentile, thus showing about 10 000 over-lake event-peaks. Future precipitation return levels from pure Clausius–Clapeyron considerations are estimated by the green dashed–dotted line, applying 7 % K^{-1} scaling with 2.4 K over-lake mean near-surface temperature increase. Data is produced by two 10-year COSMO-CLM simulations, covering the periods 2006–2015 and 2081–2090, the latter applying the pseudo global warming approach.

A stronger dependence is observed when binning the time series according to wind gust event-peaks and visualizing their corresponding precipitation intensity distribution (Fig. 3c). Severe wind gusts show >33% chance of being accompanied by intense precipitation that exceeds 28.0 mm/h (Fig. 3d). This is substantially higher than ~5% intense precipitation chance given a moderate 15 m/s wind gust event-peak. Future chances of co-occurrence are slightly higher (6%–58% relative increase) for each bin.

In addition, the bivariate distribution (black contour lines) as well as the relative change (background colors) of over-lake extreme event-peaks are given (Fig. 4). From the contour lines, it is clear that more than 90% of the over-lake model output shows no or very limited rainfall amount, in combination with moderate wind gusts (<20 m/s). Contour lines for present-day extreme events are drawn up to the 99.9999th percentile, including events with rainfall intensities up to ~110 mm/h and wind gusts up to ~40 m/s. This outermost contour

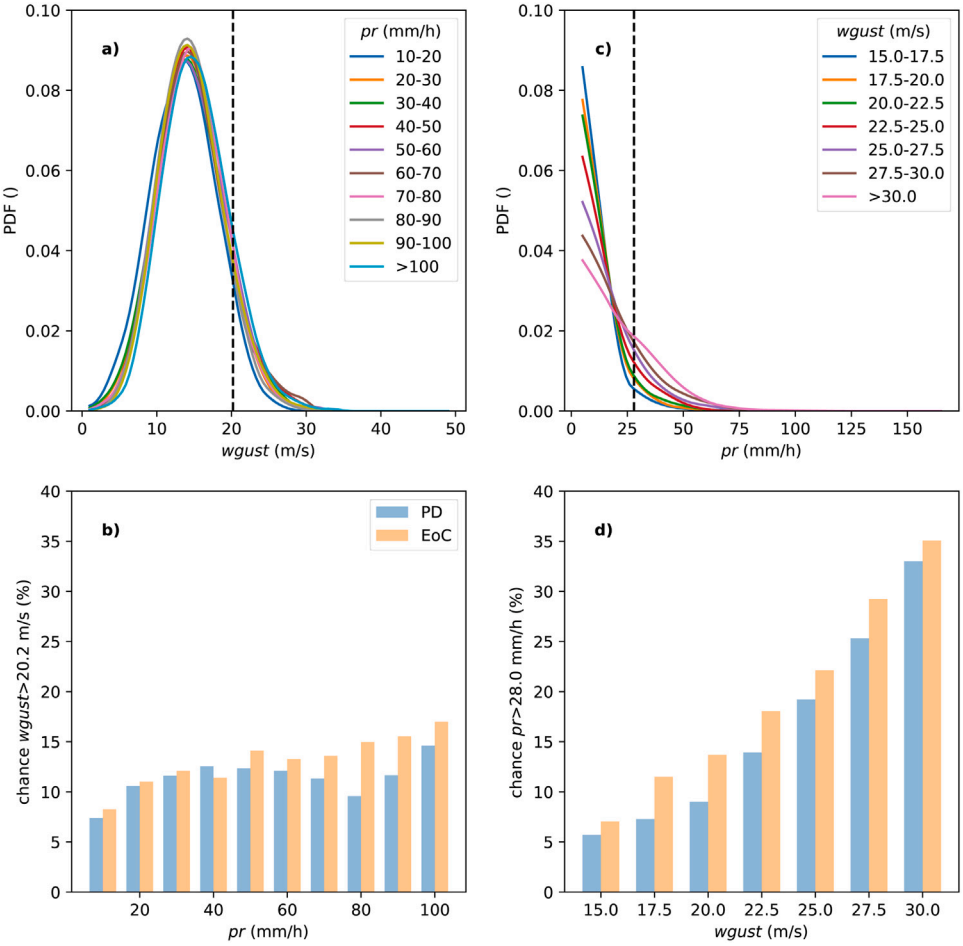

Fig. 3. Dependence analysis between precipitation and wind gust extremes over Lake Victoria, based on two 10-year COSMO-CLM simulations, covering the periods 2006–2015 and 2081–2090, the latter applying the pseudo global warming approach. (a) For binned rainfall intensities, the present-day probability density function (PDF) for maximal hourly wind gust is given, after which (b) the chances of exceeding 20.2 m/s is retrieved and compared against the end-of-century chances. (c and d) The same procedure is repeated while binning wind gust events, using the 28.0 mm/h threshold which one million event-peaks exceed.

line is missing the approximately 1000 most extreme hourly event-peaks. Bivariate events are binned according to present-day percentiles and relative changes are computed. All extreme precipitation events are clearly intensifying, for example, intense 'precipitation only' events occur up to three times more frequently. Yet, compound thunderstorms accompanied by both intense precipitation and strong wind gusts have the largest relative change, up to a factor 18 for the most extreme bin. The number of severe 'wind gusts only' events barely changes, with similar ~25 m/s and slight increase of >30 m/s event-peaks, confirming the result from the return level analysis (Fig. 2b).

3.3. Atmospheric thunderstorm drivers

Specific atmospheric conditions and complex interactions influence the formation of thunderstorms. Explaining the mean over-lake precipitation starts with the mean near-surface air temperature, for which a clear warming is projected over the Lake Victoria region (Fig. 5). While comparing simulations of 10 years of present-day climate with 10 years of end-of-century climate, the domain-averaged near-surface temperature increase is 3.5 K under a high-emission scenario. However, this projected temperature increase is strongly heterogeneous. The mean over-lake near-surface temperature change is only 2.4 K, due to the lagged lake water response to warming and other thermodynamic effects (Joshi et al., 2008; Thiery et al., 2016; Byrne and O'Gorman, 2018). Moreover, this spatially unequal warming is amplified by a temporally unequal warming of Lake Victoria's surrounding land, experiencing a stronger nighttime than daytime warming of 4.2 K and 3.0 K, respectively. The pronounced reduction in nighttime temperature contrast in future can weaken the nighttime land breeze, as visualized by the 10 m wind arrows in Fig. 5a–c, which often forms the necessary trigger for over-lake nighttime thunderstorm initiation (Docquier et al., 2016; Thiery et al., 2017; Woodhams et al., 2019; Van de Walle et al., 2020). Indeed, this weakening land breeze effect overbalances the 1–2%K^{-1} mean precipitation scaling expected from the mean column-integrated atmospheric moisture content (*TQV*, as shown later in Fig. 7a–c), which strongly increases by the end of the century. Despite the increased moisture content, the mean nighttime rainfall is even projected to decrease over a large part of Lake Victoria due to the weakened land breeze (Fig. 6a–c), consistent with coarse-scale ensemble projections (Souverijns et al., 2016). No change is observed in daytime over-lake precipitation, as subsiding air systematically suppresses deep cloud formation in both present-day as end-of-century simulations (Van de Walle et al., 2020). Over Lake Victoria's surrounding land, an increase of both day- and nighttime rainfall is projected.

Besides a weaker lake-induced circulation and higher moisture content, an overall increase of mean mixed-layer CAPE is observed, with largest changes over the lake (Fig. 7d–f). This parameter is often used as estimator for theoretically maximal updraft velocity (Fig. 7g–i). However, the explicit representation of convection and the high number of vertical model layers allow us to calculate the actual maximal vertical updraft speed, showing only a very weak, mainly positive signal over the lake. In addition, while average land CIN increases, the over-lake change is small (Fig. 7j–l). Lastly, mean maximal wind

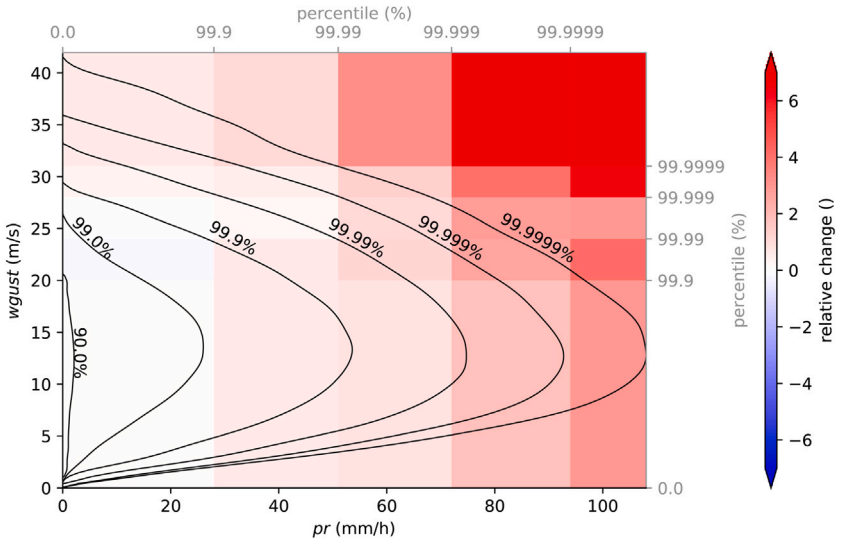

Fig. 4. Bivariate precipitation and wind gust frequency distribution of over-lake extreme events (black contours), based on the present-day COSMO-CLM simulation, covering the period 2006–2015. The indicated percentages refer to the percentage of present-day conditions enclosed by the corresponding contour line. The background colors represent relative change of events towards the end of the century (2081–2090). All events are split into classes based on their univariate occurrence as shown by the percentiles at the top and right axes. (For interpretation of the references to color in this figure legend, the reader is referred to the web version of this article.)

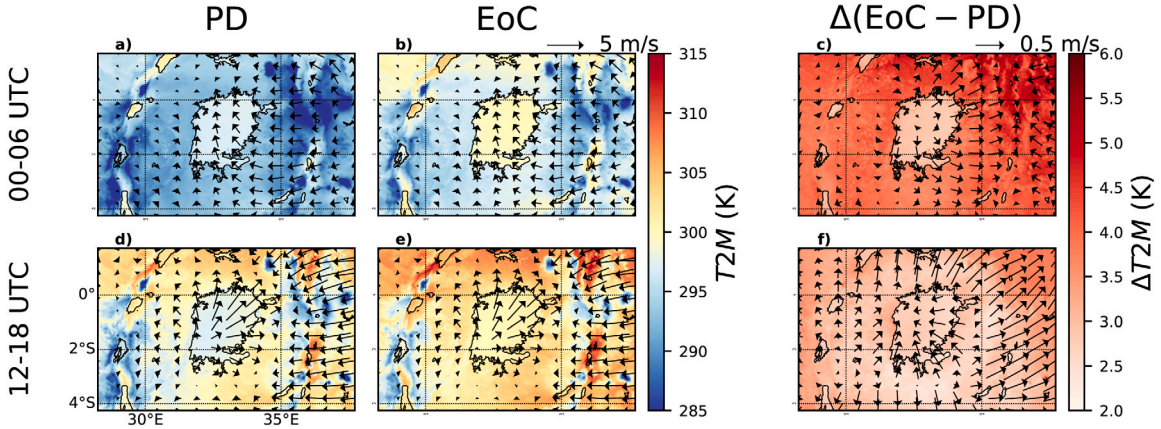

Fig. 5. Present-day (PD) and end-of-century (EoC) night- and daytime near-surface temperature averages, as well as mean 10 m wind vectors. Absolute differences are included in the right column, showing both temperature and wind changes. Data is produced by two 10-year COSMO-CLM simulations, covering the periods 2006–2015 and 2081–2090, the latter applying the pseudo global warming approach.

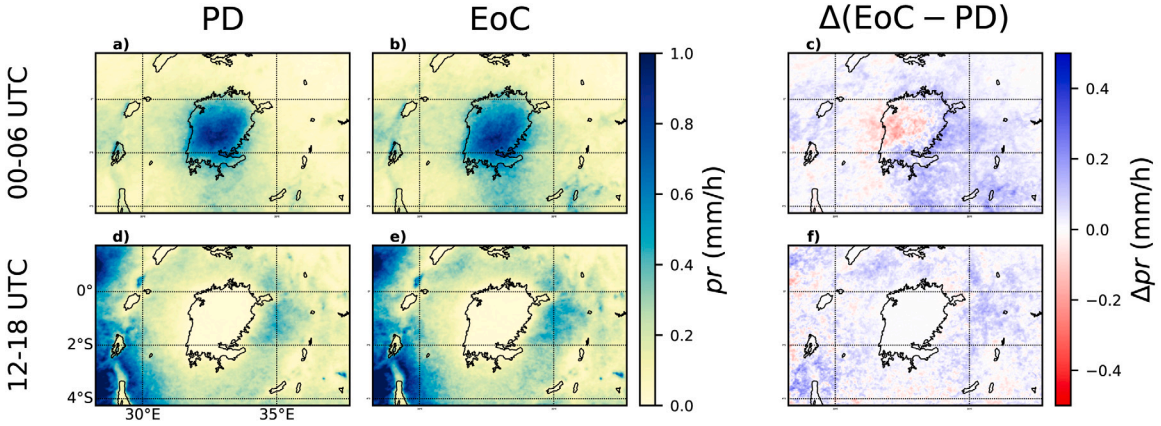

Fig. 6. Present-day (PD) and end-of-century (EoC) night- and daytime hourly precipitation averages. Absolute differences are included in the right column. Data is produced by two 10-year COSMO-CLM simulations, covering the periods 2006–2015 and 2081–2090.

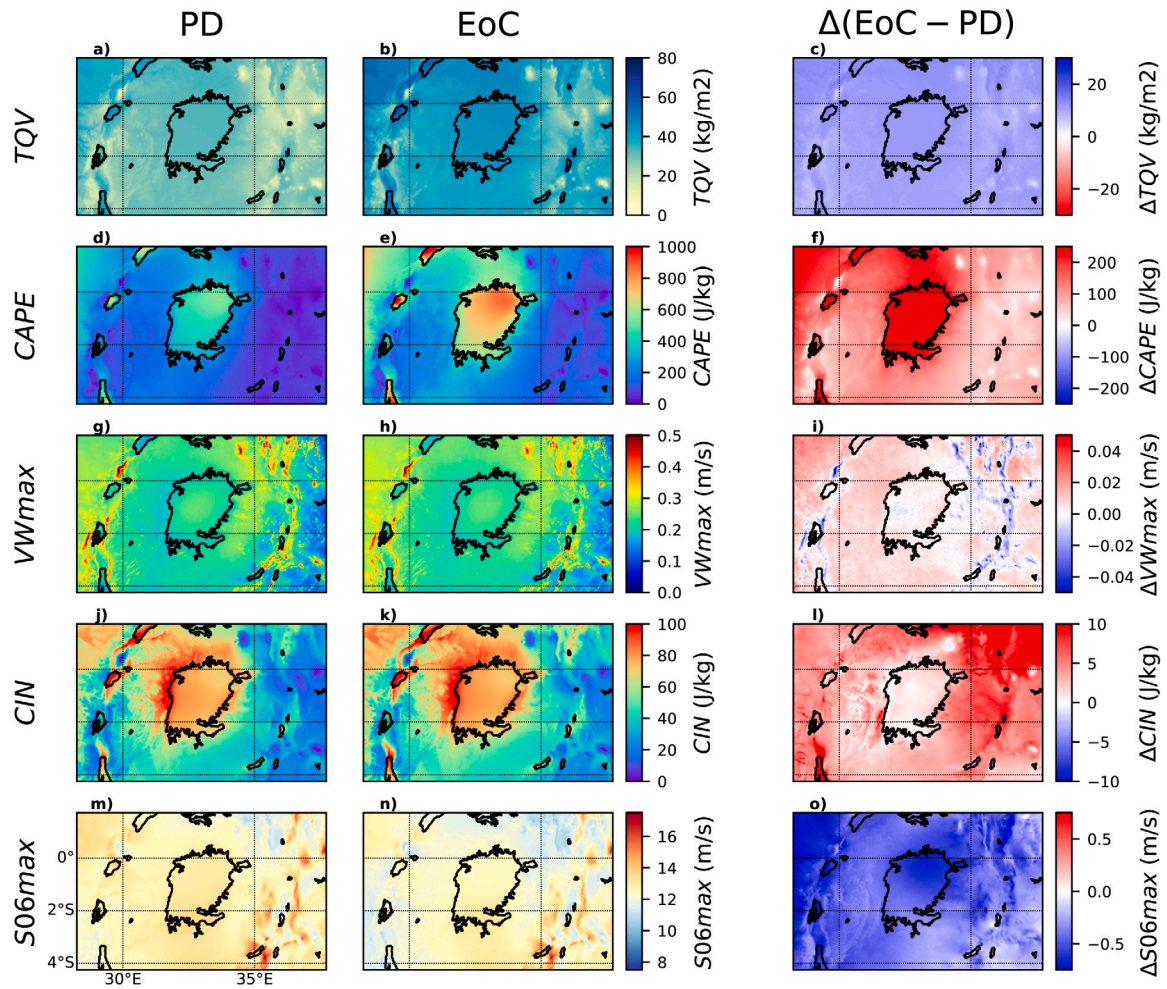

Fig. 7. Present-day (PD) and end-of-century (EoC) averaged fields for thunderstorm-preceding important variables: column-integrated water vapor content (TQV), convection available potential energy ($CAPE$), maximal vertical wind speed ($VWmax$), convective inhibition (CIN) and maximal wind shear below 6 km height ($S06max$). Absolute differences are included in the right column. Note the reversed colorscale for TQV. Data is produced by two 10-year COSMO-CLM simulations, covering the periods 2006–2015 and 2081–2090, the latter applying the pseudo global warming approach. (For interpretation of the references to color in this figure legend, the reader is referred to the web version of this article.)

shear below 6 km height is often proposed as an important driver for severe thunderstorms with strong wind gusts (Brooks et al., 2003; Trapp et al., 2007; Muller, 2013; Taylor et al., 2017; Púčik et al., 2017). It decreases throughout the entire domain, with largest changes over the Congo basin, the northern half of Lake Victoria and its northeastern shores (Fig. 7m–o). Besides large-scale synoptic wind changes in this region, the maximal wind shear is partly determined by mesoscale wind systems, such as Lake Victoria's lake/land breezes with corresponding return flows higher up. Weakened breezes in future could therefore lead to the weakened shear.

The most important atmospheric conditions that drive precipitation and wind gusts over Lake Victoria are analyzed in more detail, with particular attention given to conditions leading to extremes (Fig. 8). All values are binned according to the rainfall intensity and wind gust strength, respectively the left and right column in the figure, and plotted in blue. Specific selections are represented in orange. First, focusing on precipitation (Fig. 8, left column), the maximal updraft ($VWmax$, Fig. 8a) preceding intense rainfall is strong, reaching mean values of ~27 m/s. This is independent of the co-occurrence of severe wind gusts (orange curve). The presence of wind shear ($S06max$, Fig. 8c) has little effect on the rainfall intensity, yet more (less) intense rainfall is sometimes related to slightly stronger (weaker) wind shear. Column-integrated water vapor (TQV, Fig. 8e) is, unsurprisingly, an important driver for precipitation, independent of wind gust co-occurrence. In addition, positive over-lake mass flux convergence at 850 hPa ($lakeMFC850$, Fig. 8g) is favorable for thunderstorm initiation, with high values clearly beneficial to produce intense rainfall.

The second column of Fig. 8 investigates drivers for wind gusts. While barely important for explaining precipitation intensity, pronounced wind shear conditions are favorable for severe wind gusts (Fig. 8d). Both vertical updraft and column-integrated water vapor content also show a positive dependency on the wind gust strength, except for the high-rainfall selection for column-integrated water vapor (Fig. 8b,f). The all-case blue curve is generally below the high-rainfall selection (orange) curve. Remarkably, the blue all-case curve crosses and even overtakes the high-rainfall selection for vertical updraft and column-integrated water vapor content, possibly explained by wind gusts that require a dry atmospheric layer underneath the thunderstorm to produce evaporation-driven downdrafts. Though generally smaller than for precipitation, severe wind gusts also require positive over-lake mass flux convergence (Fig. 8h).

This univariate analysis allowed selecting most relevant atmospheric drivers. Yet, a multivariate approach is recommended (i) to gain insight into the combined drivers resulting in extreme and compound

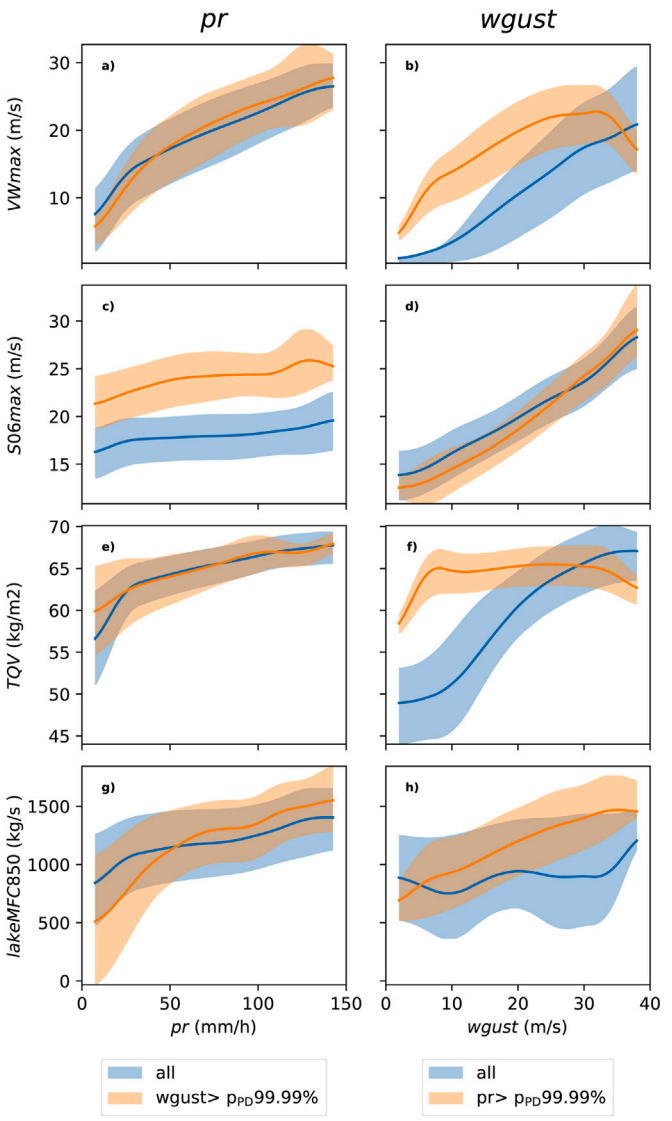

Fig. 8. Present-day dependency of precipitation intensity and wind gust strength over Lake Victoria on the thunderstorm-preceding atmospheric drivers maximal vertical wind speed ($VWmax$), maximal wind shear below 6 km height ($S06max$), column-integrated water vapor content (TQV) and over-lake mass flux convergence at 850 hPa ($lakeMFC850$) (Blue curves). Orange curves are the same, but analysis is restricted to extreme wind gust or precipitation exceeding the present-day 99.99th percentile. The full line represents the running average, lower and upper limits of the shaded areas are the 25th and 75th running quantiles. Running windows have a width of 7 mm/h and 5 m/s for precipitation and wind gusts, respectively. (For interpretation of the references to color in this figure legend, the reader is referred to the web version of this article.)

events (Zscheischler et al., 2018, 2020), (ii) to investigate changes of these combined drivers towards the end of the century and hence (iii) to explain projected rainfall and wind gust changes. Therefore, two bivariate plots are created, first combining vertical updraft and wind shear (Fig. 9). The by far most frequent over-lake atmospheric situation consists of near-zero vertical movement and moderate wind shear (~13 m/s). In about 1% of the time, the atmosphere becomes unstable with upward motions exceeding 10 m/s. For about 10 times per year, the vertical wind speed exceeds 35 m/s. Also wind shear can deviate from its most common situation, reaching values above 40 m/s about 60 times per year. Bivariate conditions producing most present-day hazards (extreme precipitation, extreme wind gusts, or both) are enclosed by contour lines. Extreme hourly 'precipitation only' event-peaks, characterized by rainfall amounts exceeding 72 mm/h (the 99.999th present-day percentile) and wind gusts below 10 m/s, are centered around ~12 m/s vertical updraft and moderate wind shear (~15 m/s). Different conditions, namely near-zero vertical updraft but relatively strong wind shear, produce the most 'wind gust only' events, characterized by gusts exceeding 28 m/s (the 99.999th present-day percentile) and below 1 mm/h rainfall. Compound extreme events with both intense precipitation and severe wind gusts within a 5-hourly time period, are produced by both very strong updraft and wind shear conditions. These conditions could be favorable to produce supercell thunderstorms characterized by rotating updrafts.

Clear changes are projected for both drivers (Fig. 9d–f). Updraft velocities generally increase. The largest relative increases (>100%) are observed for ~25 m/s updraft velocities, favoring the generation of compound thunderstorms. Also the occurrence of 10–15 m/s vertical updraft increases, containing the atmospheric conditions producing most 'precipitation only' extremes. For most common low updrafts, the projected wind shear shows a remarkable shift from above-average (>~13 m/s) to below-average (<~13 m/s). Assuming wind shear often originates from mesoscale circulation over Lake Victoria, this shift is possibly explained by the weakening circulation in the Lake Victoria region (see Fig. 5). The combination of decreasing above-average shear occurrence at near-zero updraft and the slightly increasing occurrences of small positive updrafts, both enclosed by the 'wind gust only' (green) contours, explain the unchanged number of such extremes in the end-of-century simulation.

A second bivariate plot visualizes 850 hPa over-lake mass flux convergence against maximal updraft velocity (Fig. 10). Both present-day absolute frequencies and end-of-century relative changes are considered, while focusing again on the conditions producing extremes. The over-lake mass flux convergence shows both negative and positive contributions, corresponding with daytime diverging and nighttime converging low-level winds, respectively. However, the positive contribution is clearly larger, resulting in a positive mean (~500 kg/s). Since both variables are likely not independent, positive over-lake mass flux convergence conditions frequently co-occur with unstable conditions and large updrafts. Most extremes are triggered by low-level convergence, though some exceptional 'wind gust only' events are present in over-lake diverging conditions.

Relative changes in over-lake mass flux convergence are remarkable (Fig. 10d–f). Moderate negative flux occurrence substantially increases, while moderate positive flux only occurs more often in combination with sufficiently strong updraft conditions. The frequency of small positive and small to moderate negative fluxes increase at the expense of strong divergence (<−1500 kg/s) and moderate to strong convergence (>500 kg/s) conditions, as expected by the lake-land temperature contrast changes during day- and nighttime (see Fig. 5). This overall reduction of over-lake mass flux convergence implies less thunderstorm triggering. At the same time, stronger updrafts intensify precipitation events, thereby compensating the initiation reduction. This compensating effect for rainfall-associated extremes is clear from Fig. 10e, showing that the extreme contours contain both the decreasing frequency of strong converging conditions and the increasing frequency of positive moderate converging conditions with strong updrafts.

4. Discussion and conclusion

Though literature proposes a global mean precipitation increase of 1–3% per degree warming (Allen and Ingram, 2002; Held and Soden, 2006; Westra et al., 2014), particular circumstances make the Lake Victoria basin deviate from this commonly accepted scaling. Instead, over-lake mean precipitation is projected to even decrease towards the end of the century in our convection-permitting regional climate simulations, due to an unequal lake-land warming, weakened nightly land breeze strength and consequently reduced thunderstorm triggering. With this generally weaker trigger mechanism, one could also expect a decreased frequency of intense rainfall. Yet, our results

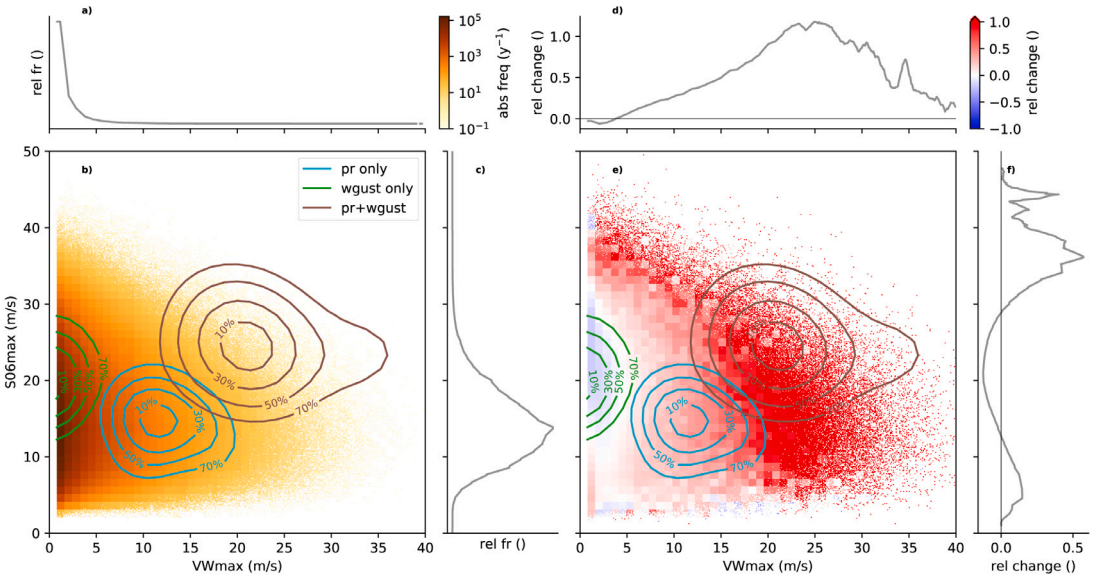

Fig. 9. Bivariate absolute frequency of co-occurring wind shear (*S06max*) and vertical wind speed (*VWmax*) atmospheric drivers (b), as well as their univariate relative fractions (a,c). Bin sizes of 1 m/s are chosen for both variables, while a finer 0.1 m/s mask filters out non-existing conditions in the present-day simulation. Contour lines show the contributions of these drivers to 'precipitation-only', 'wind gust only' and compound thunderstorm events over Lake Victoria. The right panel shows the bivariate relative changes of both drivers (e) with corresponding univariate relative changes (d,f). Contour lines from the left panel are copied. Data is produced by two 10-year COSMO-CLM simulations, covering the periods 2006–2015 and 2081–2090, the latter applying the pseudo global warming approach.

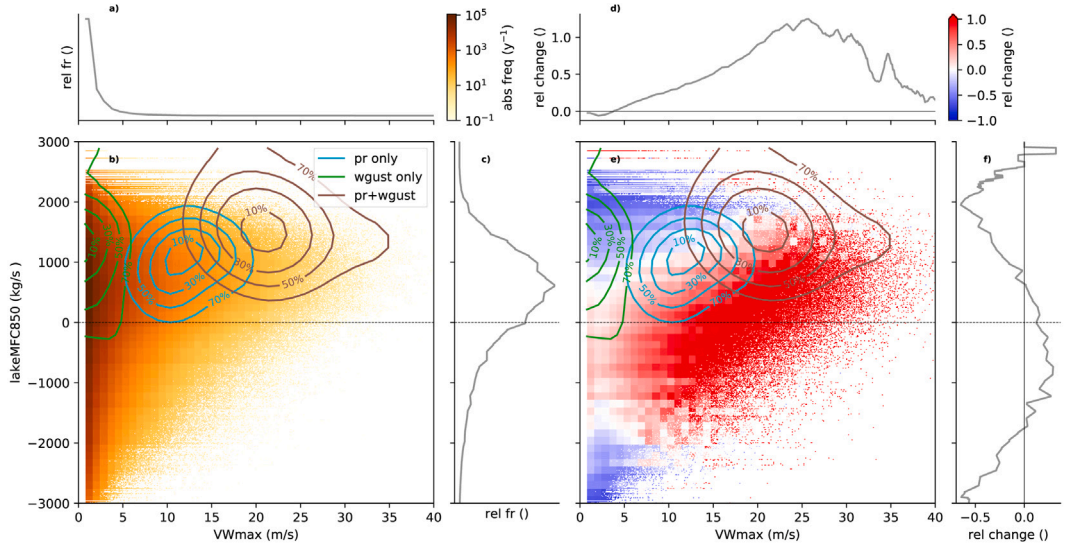

Fig. 10. Bivariate absolute frequency of co-occurring over-lake mass flux convergence (*lakeMFC850*) and vertical wind speed (*VWmax*), as well as their univariate relative fractions (a–c). Bin sizes of 1 m/s are chosen for both variables, while a finer 0.1 m/s mask filters out non-existing conditions in the present-day simulation. Contour lines show the contributions of these drivers to 'precipitation only', 'wind gust only' and compound thunderstorm events over Lake Victoria. The right panel shows the bivariate changes of both drivers (e) with corresponding univariate relative changes (d,f). Contour lines from the left panel are copied. Data is produced by two 10-year COSMO-CLM simulations, covering the periods 2006–2015 and 2081–2090, the latter applying the pseudo global warming approach.

highlight an increased intense rainfall frequency closely following the Clausius–Clapeyron scaling, corroborating former studies over the region (Kendon et al., 2019; Finney et al., 2020). We find that the decreased trigger mechanism is actually compensated by strengthened thunderstorm dynamics, seen by increased maximal vertical updraft speed. This was hypothesized already by former literature focusing on CAPE, the environmental proxy for thunderstorm dynamics (Muller et al., 2011; Romps, 2016; Rasmussen et al., 2020).

The projected weaker mesoscale circulation not only affects over-lake precipitation, it also influences the thunderstorm organization and related wind gust occurrence. In particular, the total circulation includes both the near-surface breeze as well as its corresponding opposite return flow (Thiery et al., 2015; Woodhams et al., 2021). Together with large-scale wind changes, this mesoscale combined flow determines the maximal wind shear below 6 km height. Though the weakening mesoscale circulation is specific for the Lake Victoria region, the resulting wind shear reduction agrees with projections for other regions worldwide (Allen et al., 2014; Seeley and Romps, 2015a; Púčik et al., 2017). Generally, wind shear can largely affect the wind gust severeness (Trapp et al., 2007; Trapp and Hoogewind, 2016). Our results confirm this relation over Lake Victoria. Moreover, it also explains the decrease in mean wind gust severeness. Despite this overall decrease, severe wind gusts exceeding 30 m/s tend to intensify in future, shown to be statistically significant, except for the highest return periods (>1y). To statistically identify whether these most severe wind gusts also intensify in the future or not, longer simulation periods are

recommended to reduce the uncertainty on such high return levels. Would the wind gust intensification be an actual climate change-induced signal, we ascribe it to the large increase in relative frequency of compound precipitation-wind gust extremes. We hypothesize that such compound events possibly result from rain, graupel and hail fall-out that, enhanced by evaporatively cooled downdrafts, produce downbursts and wind gusts (Markowski and Richardson, 2011; Zinner and Groenemeijer, 2012). Importantly, while the compound extremes clearly have the highest relative increase, their occurrence is still low. This might question their contribution to the overall risk of capsizing accidents on Lake Victoria.

To explain changes of compound events, future research could investigate the vertical moisture distribution in the atmosphere preceding thunderstorms, as well as the maximal downdraft velocity, often represented by the downdraft CAPE environmental proxy (Molinari et al., 2013). Another hypothesis reads that compound events occur in highly organized thunderstorms, which are favored by wind shear driven unstable atmospheres (Doswell, 2001). In contrast, 'precipitation only' events are formed in unstable atmospheres with weak wind shear, probably produced by unorganized, slow-moving single-cell thunderstorms. In addition, the origin of some 'wind gust only' events with near-zero maximal updraft speed, is uncertain but possibly related to outflows from thunderstorms further away.

Thunderstorm organization is only indirectly investigated by assuming it is largely affected by wind shear. Though this assumption is commonly accepted (Muller, 2013), many uncertainties about organization effects on precipitation and wind gusts remain. Following Prein et al. (2017a), applying a storm-tracking algorithm to the high-resolution simulation output and satellite data could allow to distinguish single cell events from organized events such as Mesoscale Convective Systems, shown to significantly contribute to Lake Victoria's total precipitation (Nesbitt et al., 2006; Nicholson et al., 2021). Besides providing insight into structured events over Lake Victoria, future changes can be investigated explicitly and aforementioned hypotheses can be tested. As an additional advantage, such storm-tracking approach can improve the definition of an event by accounting for the storm size and duration. Here, environmental conditions are spatially averaged over a radius of 14 km around the event-peak, but this radius should obviously be variable. In addition, environmental conditions are temporally maximized over 3 h preceding the event-peak, which can be too short for long-lasting storms.

Besides the importance of thunderstorm organization, future research should also confirm the origin of decreased wind shear over the lake. In this work, this decrease was assumed to be caused by a reduced mesoscale circulation, neglecting possible large-scale changes. However, as a consequence of our pseudo global warming approach which applies the CMIP6 multi-model mean change to the reanalysis lateral boundary conditions, large-scale dynamical changes are small, whereas some members do project changing dynamics in the future. In a first stage, this average forcing is advantageous, as it removes high uncertainty of changes in atmospheric dynamics as reflected by the different CMIP6 members. However, individual ensemble members might project important future wind shear changes. Associated changes in large-scale dynamics could also alter the moisture inflow over Lake Victoria, affecting precipitation totals and extremes. Moreover, blocking effects of easterly trade winds by high mountains influence the rainfall location (Docquier et al., 2016; Van de Walle et al., 2020), possibly leading to additional changes. This will be investigated in a future study, where the effect of changing atmospheric circulation from CMIP6 members will be studied.

In the end, the major risk at Lake Victoria arises from strong waves capsizing fisher boats, passenger ferries and goods transport boats. Such waves are assumed to be associated with heavy thunderstorms and severe wind gusts. Previous studies that investigated that particular risk exclusively focused on rainfall extremes, thereby assuming a direct relation between intense precipitation, severe wind gusts, and eventually high waves (Chamberlain et al., 2014; Thiery et al., 2016; Woodhams et al., 2019; Finney et al., 2020). However, here we show that many intense precipitation events are not associated with severe wind gusts, and that the future intensification of precipitation events is much stronger than the increase of severe wind gust occurrence. Therefore, an estimation based on precipitation extremes only can substantially overestimate the future wave-related risk at Lake Victoria. Even though a direct wind gust investigation removes one assumption for a proper risk assessment, it still assumes that waves are produced during windy conditions. The retrieval of raw wave properties from a coupled atmosphere-wave model over Lake Victoria would open new doors. Such coupling has been successfully accomplished for oceans and inland waters worldwide (Lalbeharry et al., 2000; Cavaleri et al., 2007; Seibt et al., 2013; Aijaz et al., 2016; Wahle et al., 2017; Shanas et al., 2017; Porchetta et al., 2020), but Lake Victoria's stormy weather could push the model possibilities to the limit, while the lack of in-situ wave-related measures can complicate the evaluation.

CRediT authorship contribution statement

Jonas Van de Walle: Conceptualization, Methodology, Software, Formal analysis, Writing - original draft. **Wim Thiery:** Conceptualization, Methodology, Writing - review & editing, Supervision. **Roman Brogli:** Methodology, Software, Writing - review & editing. **Olivia Martius:** Methodology, Writing - review & editing. **Jakob Zscheischler:** Methodology, Writing - review & editing. **Nicole P.M. van Lipzig:** Conceptualization, Methodology, Writing - review & editing, Supervision.

Declaration of competing interest

The authors declare that they have no known competing financial interests or personal relationships that could have appeared to influence the work reported in this paper.

Acknowledgments

This work was financially supported by internal KU Leuven Internal Special Research Fund (Belgium) (BOF-C1 project C14/17/053). J.Z. acknowledges the Swiss National Science Foundation (Switzerland) (Ambizione grant 179876) and the Helmholtz Initiative and Networking Fund (Germany) (Young Investigator Group COMPOUNDX, Grant Agreement VH-NG-1537). The authors would like to thank the European COST Action DAMOCLES (Europe). Special thanks to Sonia Seneviratne and Dominik Michel (ETHZ) for providing the weather station data from Nkose Island (Uganda). We would also like to express our gratitude to the European Centre for Medium-Range Weather Forecasts (ECMWF) for providing the ERA5 reanalysis data and to the COSMO-CLM community (http://www.clm-community.eu) for their efforts in both providing the model source code and helping to post-process ERA5 data. This data has been downloaded with the help of the German Climate Compute Centre (DKRZ) infrastructure, while the computational resources and services used in this work were mainly enabled by the Flemish Supercomputing Center (VSC). CMIP6 data used in this study was downloaded from the ESGF nodes via https://esgf-data.dkrz.de/projects/esgf-dkrz/, latest access 29-11-2019. The dataset generated under this project can be obtained by contacting the first author.

Appendix A. Supplementary data

Supplementary material related to this article can be found online at https://doi.org/10.1016/j.wace.2021.100391.

References

Abdalla, S., Cavaleri, L., 2002. Effect of wind variability and variable air density on wave modeling. J. Geophys. Res. Oceans 107 (C7), 17-1–17-17.

Aijaz, S., Rogers, W.E., Babanin, A.V., 2016. Wave spectral response to sudden changes in wind direction in finite-depth waters. Ocean Model. 103, 98–117.

Akkermans, T., Thiery, W., Van Lipzig, N.P., 2014. The regional climate impact of a realistic future deforestation scenario in the Congo Basin. J. Clim. 27 (7), 2714–2734.

Allan, R.P., Soden, B.J., 2008. Atmospheric warming and the amplification of precipitation extremes. Science 321 (5895), 1481–1484.

Allen, M.R., Ingram, W.J., 2002. Constraints on future changes in climate and the hydrologic cycle. Nature 419 (6903), 228–232.

Allen, J.T., Karoly, D.J., Walsh, K.J., 2014. Future Australian severe thunderstorm environments. Part II: The influence of a strongly warming climate on convective environments. J. Clim. 27 (10), 3848–3868.

Almazroui, M., Saeed, F., Saeed, S., Islam, M.N., Ismail, M., Klutse, N.A.B., Siddiqui, M.H., 2020. Projected change in temperature and precipitation over Africa from CMIP6. Earth Syst. Environ. 4 (3), 455–475.

Anyah, R.O., Semazzi, F.H., Xie, L., 2006. Simulated physical mechanisms associated with climate variability over Lake Victoria basin in East Africa. Mon. Weather Rev. 134 (12), 3588–3609.

Ban, N., Schmidli, J., Schär, C., 2015. Heavy precipitation in a changing climate: Does short-term summer precipitation increase faster? Geophys. Res. Lett. 42 (4), 1165–1172.

Berg, P., Moseley, C., Haerter, J.O., 2013. Strong increase in convective precipitation in response to higher temperatures. Nat. Geosci. 6 (3), 181–185.

Bosshard, T., Kotlarski, S., Ewen, T., Schär, C., 2011. Spectral representation of the annual cycle in the climate change signal. Hydrol. Earth Syst. Sci. 15 (9), 2777–2788. http://dx.doi.org/10.5194/hess-15-2777-2011.

Brisson, E., Van Weverberg, K., Demuzere, M., Devis, A., Saeed, S., Stengel, M., van Lipzig, N.P., 2016. How well can a convection-permitting climate model reproduce decadal statistics of precipitation, temperature and cloud characteristics? Clim. Dynam. 47 (9), 3043–3061.

Brogli, R., Kröner, N., Sørland, S.L., Lüthi, D., Schär, C., 2019. The role of Hadley circulation and lapse-rate changes for the future European summer climate. J. Clim. 32 (2), 385–404.

Brooks, H.E., 2013. Severe thunderstorms and climate change. Atmos. Res. 123, 129–138.

Brooks, H.E., Lee, J.W., Craven, J.P., 2003. The spatial distribution of severe thunderstorm and tornado environments from global reanalysis data. Atmos. Res. 67, 73–94.

Byrne, M.P., O'Gorman, P.A., 2018. Trends in continental temperature and humidity directly linked to ocean warming. Proc. Natl. Acad. Sci. 115, 4863–4868. http://dx.doi.org/10.1073/pnas.1722312115.

Cannon, T., Krüger, F., Bankoff, G., Schipper, L., Bamforth, T., 2014. Putting culture at the centre of risk reduction. In: World Disasters Report 2014: Focus on Culture and Risk. International Federation of Red Cross and Red Crescent Societies, pp. 185–209.

Cao, J., Wang, B., Young-Min, Y., Ma, L., Li, J., Sun, B., Bao, Y., He, J., Zhou, X., Wu, L., 2018. The NUIST earth system model (NESM) version 3: description and preliminary evaluation. Geosci. Model Dev. 11 (7), 2975–2993.

Cavaleri, L., Alves, J.-H., Ardhuin, F., Babanin, A., Banner, M., Belibassakis, K., Benoit, M., Donelan, M., Groeneweg, J., Herbers, T., et al., 2007. Wave modelling–the state of the art. Prog. Oceanogr. 75 (4), 603–674.

Chamberlain, J., Bain, C., Boyd, D., McCourt, K., Butcher, T., Palmer, S., 2014. Forecasting storms over Lake Victoria using a high resolution model. Meteorol. Appl. 21 (2), 419–430.

Chan, S.C., Kendon, E.J., Roberts, N.M., Fowler, H.J., Blenkinsop, S., 2016. Downturn in scaling of UK extreme rainfall with temperature for future hottest days. Nat. Geosci. 9 (1), 24–28.

Coles, S., Bawa, J., Trenner, L., Dorazio, P., 2001. An Introduction to Statistical Modeling of Extreme Values, Vol. 208. Springer.

Coppola, E., Sobolowski, S., Pichelli, E., Raffaele, F., Ahrens, B., Anders, I., Ban, N., Bastin, S., Belda, M., Belusic, D., et al., 2020. A first-of-its-kind multi-model convection permitting ensemble for investigating convective phenomena over Europe and the Mediterranean. Clim. Dynam. 55 (1), 3–34.

Del Genio, A.D., Yao, M.-S., Jonas, J., 2007. Will moist convection be stronger in a warmer climate? Geophys. Res. Lett. 34 (16).

Docquier, D., Thiery, W., Lhermitte, S., Van Lipzig, N., 2016. Multi-year wind dynamics around Lake Tanganyika. Clim. Dynam. 47 (9), 3191–3202.

Dosio, A., Panitz, H.J., 2016. Climate change projections for CORDEX-africa with COSMO-CLM regional climate model and differences with the driving global climate models. Clim. Dynam. 46 (5–6), 1599–1625. http://dx.doi.org/10.1007/s00382-015-2664-4.

Doswell, C.A., 2001. Severe convective storms—An overview. In: Severe Convective Storms. Springer, pp. 1–26.

Emori, S., Brown, S., 2005. Dynamic and thermodynamic changes in mean and extreme precipitation under changed climate. Geophys. Res. Lett. 32 (17).

Eyring, V., Bony, S., Meehl, G.A., Senior, C.A., Stevens, B., Stouffer, R.J., Taylor, K.E., 2016. Overview of the Coupled Model Intercomparison Project Phase 6 (CMIP6) experimental design and organization. Geosci. Model Dev. 9 (5), 1937–1958.

Eyring, V., Cox, P.M., Flato, G.M., Gleckler, P.J., Abramowitz, G., Caldwell, P., Collins, W.D., Gier, B.K., Hall, A.D., Hoffman, F.M., et al., 2019. Taking climate model evaluation to the next level. Nature Clim. Change 9 (2), 102–110.

Finney, D.L., Marsham, J.H., Jackson, L.S., Kendon, E.J., Rowell, D.P., Boorman, P.M., Keane, R.J., Stratton, R.A., Senior, C.A., 2019. Implications of improved representation of convection for the East Africa water budget using a convection-permitting model. J. Clim. 32 (7), 2109–2129.

Finney, D.L., Marsham, J.H., Rowell, D.P., Kendon, E.J., Tucker, S.O., Stratton, R.A., Jackson, L.S., 2020. Effects of explicit convection on future projections of mesoscale circulations, rainfall, and rainfall extremes over eastern africa. J. Clim. 33 (7), 2701–2718.

Fowler, H.J., Lenderink, G., Prein, A.F., Westra, S., Allan, R.P., Ban, N., Barbero, R., Berg, P., Blenkinsop, S., Do, H.X., et al., 2021. Anthropogenic intensification of short-duration rainfall extremes. Nat. Rev. Earth Environ. 1–16.

Gilleland, E., Katz, R.W., 2016. ExtRemes 2.0: An extreme value analysis package in R. J. Stat. Softw. 72 (1), 1–39.

Giorgi, F., Jones, C., Asrar, G.R., 2009. Addressing climate information needs at the regional level: the CORDEX framework. World Meteorol. Organ. Bull. 58 (3), 175–183. http://dx.doi.org/10.1109/ICASSP.2009.4960141.

Giorgi, F., Torma, C., Coppola, E., Ban, N., Schär, C., Somot, S., 2016. Enhanced summer convective rainfall at alpine high elevations in response to climate warming. Nat. Geosci. 9 (8), 584–589.

Grasselt, R., Schüttemeyer, D., Warrach-Sagi, K., Ament, F., Simmer, C., 2008. Validation of TERRA-ML with discharge measurements. Meteorol. Z. 17 (6), 763–773.

Gutjahr, O., Putrasahan, D., Lohmann, K., Jungclaus, J.H., von Storch, J.S., Brüggemann, N., Haak, H., Stössel, A., 2019. Max Planck institute earth system model (MPI-ESM1. 2) for high-resolution model intercomparison project (HighResMIP). Geophys. Model Dev. 12, 3241–3281.

Hardwick Jones, R., Westra, S., Sharma, A., 2010. Observed relationships between extreme sub-daily precipitation, surface temperature, and relative humidity. Geophys. Res. Lett. 37 (22).

He, B., Bao, Q., Wang, X., Zhou, L., Wu, X., Liu, Y., Wu, G., Chen, K., He, S., Hu, W., et al., 2019. CAS FGOALS-f3-L model datasets for CMIP6 historical atmospheric model intercomparison project simulation. Adv. Atmos. Sci. 36 (8), 771–778.

Held, I., Guo, H., Adcroft, A., Dunne, J., Horowitz, L., Krasting, J., Shevliakova, E., Winton, M., Zhao, M., Bushuk, M., et al., 2019. Structure and performance of GFDL's CM4. 0 climate model. J. Adv. Modelling Earth Syst. 11 (11), 3691–3727.

Held, I.M., Soden, B.J., 2006. Robust responses of the hydrological cycle to global warming. J. Clim. 19 (21), 5686–5699.

Helsen, S., van Lipzig, N.P., Demuzere, M., Broucke, S.V., Caluwaerts, S., De Cruz, L., De Troch, R., Hamdi, R., Termonia, P., Van Schaeybroeck, B., et al., 2020. Consistent scale-dependency of future increases in hourly extreme precipitation in two convection-permitting climate models. Clim. Dynam. 54 (3), 1267–1280.

Hentgen, L., Ban, N., Kröner, N., Leutwyler, D., Schär, C., 2019. Clouds in convection-resolving climate simulations over Europe. J. Geophys. Res.: Atmos. 124 (7), 3849–3870.

Hersbach, H., Bell, B., Berrisford, P., Hirahara, S., Horányi, A., Muñoz Sabater, J., Nicolas, J., Peubey, C., Radu, R., Schepers, D., Simmons, A., Soci, C., Abdalla, S., Abellan, X., Balsamo, G., Bechtold, P., Biavati, G., Bidlot, J., Bonavita, M., De Chiara, G., Dahlgren, P., Dee, D., Diamantakis, M., Dragani, R., Flemming, J., Forbes, R., Fuentes, M., Geer, A., Haimberger, L., Healy, S., Hogan, R.J., Hólm, E., Janisková, M., Keeley, S., Laloyaux, P., Lopez, P., Lupu, C., Radnoti, G., de Rosnay, P., Rozum, I., Vamborg, F., Villaume, S., Thépaut, J.-N., 2020. The ERA5 global reanalysis. Q. J. R. Meteorol. Soc. 146 (730), 1999–2049. http://dx.doi.org/10.1002/qj.3803.

Joshi, M.M., Gregory, J.M., Webb, M.J., Sexton, D.M.H., Johns, T.C., 2008. Mechanisms for the land/sea warming contrast exhibited by simulations of climate change. Clim. Dynam. 30, 455–465. http://dx.doi.org/10.1007/s00382-007-0306-1.

Kawase, H., Yoshikane, T., Hara, M., Kimura, F., Yasunari, T., Ailikun, B., Ueda, H., Inoue, T., 2009. Intermodel variability of future changes in the baiu rainband estimated by the pseudo global warming downscaling method. J. Geophys. Res.: Atmos. 114 (D24).

Kendon, E.J., Stratton, R.A., Tucker, S., Marsham, J.H., Berthou, S., Rowell, D.P., Senior, C.A., 2019. Enhanced future changes in wet and dry extremes over Africa at convection-permitting scale. Nature Commun. 10 (1), 1–14.

Kharin, V.V., Zwiers, F.W., Zhang, X., Hegerl, G.C., 2007. Changes in temperature and precipitation extremes in the IPCC ensemble of global coupled model simulations. J. Clim. 20 (8), 1419–1444.

Kharin, V.V., Zwiers, F., Zhang, X., Wehner, M., 2013. Changes in temperature and precipitation extremes in the CMIP5 ensemble. Clim. Change 119 (2), 345–357.

Kiwanuka-Tondo, J., Semazzi, F., Pettiway, K., Casadevall, S.R., 2019. Climate risk communication of navigation safety and climate conditions over Lake Victoria basin: Exploring perceptions and knowledge of indigenous communities. Cogent Soc. Sci. 5 (1), 1588485.

Kröner, N., Kotlarski, S., Fischer, E., Lüthi, D., Zubler, E., Schär, C., 2017. Separating climate change signals into thermodynamic, lapse-rate and circulation effects: theory and application to the European summer climate. Clim. Dynam. 48 (9–10), 3425–3440.

Lalbeharry, R., Mailhot, J., Desjardins, S., Wilson, L., 2000. Examination of the impact of a coupled atmospheric and ocean wave system. Part II: Ocean wave aspects. J. Phys. Oceanogr. 30 (2), 402–415.

Lauritzen, P.H., Nair, R.D., Herrington, A., Callaghan, P., Goldhaber, S., Dennis, J., Bacmeister, J., Eaton, B., Zarzycki, C., Taylor, M.A., et al., 2018. NCAR release of CAM-SE in CESM2. 0: A reformulation of the spectral element dynamical core in dry-mass vertical coordinates with comprehensive treatment of condensates and energy. J. Adv. Modelling Earth Syst. 10 (7), 1537–1570.

Lemos, I.P., Lima, A.M.G., Duarte, M.A.V., 2020. Thresholdmodeling: A Python package for modeling excesses over a threshold using the Peak-Over-Threshold Method and the Generalized Pareto Distribution. J. Open Source Softw. 5 (46), 2013.

Li, L., 2019. CAS FGOALS-G3 Model Output Prepared for CMIP6 Scenariomip ssp370. Earth System Grid Federation, http://dx.doi.org/10.22033/ESGF/CMIP6.3480.

Li, Q., Bou-Zeid, E., Vercauteren, N., Parlange, M., 2018. Signatures of air–wave interactions over a large lake. Bound.-Lay. Meteorol. 167 (3), 445–468.

Liu, C., Ikeda, K., Rasmussen, R., Barlage, M., Newman, A.J., Prein, A.F., Chen, F., Chen, L., Clark, M., Dai, A., et al., 2017. Continental-scale convection-permitting modeling of the current and future climate of North America. Clim. Dynam. 49 (1–2), 71–95.

Markowski, P., Richardson, Y., 2011. Mesoscale Meteorology in Midlatitudes, Vol. 2. John Wiley & Sons, p. 424.

Massonnet, F., Ménégoz, M., Acosta, M., Yepes-Arbós, X., Exarchou, E., Doblas-Reyes, F.J., 2020. Replicability of the EC-Earth3 earth system model under a change in computing environment. Geosci. Model Dev. 13 (3).

Mironov, D., Heise, E., Kourzeneva, E., Ritter, B., Schneider, N., Terzhevik, A., 2010. Implementation of the lake parameterisation scheme FLake into the numerical weather prediction model COSMO. Boreal Environ. Res. Publ. Board 15, 218–230, URL https://helda.helsinki.fi/bitstream/handle/10138/233087/ber15-2-218.pdf?sequence=1.

Mironov, D., Raschendorfer, M., 2001. Evaluation of Empirical Parameters of the New LM Surface-Layer Parameterization Scheme. Tech. rep., Tech. rep., COSMO Tech. Rep. 1, p. 12, URL http://www.cosmo-model.org/content/model/documentation/techReports/docs/techReport01.pdf.

Molinari, J., Frank, J., Vollaro, D., 2013. Convective bursts, downdraft cooling, and boundary layer recovery in a sheared tropical storm. Mon. Weather Rev. 141 (3), 1048–1060.

Muller, C., 2013. Impact of convective organization on the response of tropical precipitation extremes to warming. J. Clim. 26 (14), 5028–5043.

Muller, C.J., O'Gorman, P.A., Back, L.E., 2011. Intensification of precipitation extremes with warming in a cloud-resolving model. J. Clim. 24 (11), 2784–2800.

Nesbitt, S.W., Cifelli, R., Rutledge, S.A., 2006. Storm morphology and rainfall characteristics of TRMM precipitation features. Mon. Weather Rev. 134 (10), 2702–2721.

Nicholson, S.E., Klotter, D., Hartman, A.T., 2021. Lake-effect rains over Lake Victoria and their association with Mesoscale Convective Systems. J. Hydrometeorol..

Nikulin, G., Jones, C., Giorgi, F., Asrar, G., Büchner, M., Cereso-Mota, R., Christensen, O.B., Déqué, M., Fernandez, J., Hänsler, A., Van Meijgaard, E., Samuelsson, P., Sylla, M.B., Sushama, L., 2012. Precipitation climatology in an ensemble of CORDEX-Africa regional climate simulations. J. Clim. 25 (18), 6057–6078. http://dx.doi.org/10.1175/jcli-d-11-00375.1.

O'Gorman, P.A., 2012. Sensitivity of tropical precipitation extremes to climate change. Nat. Geosci. 5 (10), 697–700.

O'Gorman, P.A., 2015. Precipitation extremes under climate change. Curr. Clim. Change Rep. 1 (2), 49–59.

O'Gorman, P., Muller, C., 2010. How closely do changes in surface and column water vapor follow Clausius–Clapeyron scaling in climate change simulations? Environ. Res. Lett. 5 (2), 025207.

Otto, F.E., Allen, M., Stott, P., van Oldenborgh, G., Eden, J., Karoly, D., 2016. Framing the question of attribution of extreme weather events. Nature Clim. Change 6.

Porchetta, S., Temel, O., Warner, J.C., Muñoz Esparza, D., Monbaliu, J., van Beeck, J., van Lipzig, N., 2020. Evaluation of a roughness length parametrization accounting for wind–wave alignment in a coupled atmosphere–wave model. Q. J. R. Meteorol. Soc..

Prein, A.F., Langhans, W., Fosser, G., Ferrone, A., Ban, N., Goergen, K., Keller, M., Tölle, M., Gutjahr, O., Feser, F., et al., 2015. A review on regional convection-permitting climate modeling: Demonstrations, prospects, and challenges. Rev. Geophys. 53 (2), 323–361.

Prein, A.F., Liu, C., Ikeda, K., Trier, S.B., Rasmussen, R.M., Holland, G.J., Clark, M.P., 2017a. Increased rainfall volume from future convective storms in the US. Nature Clim. Change 7 (12), 880–884.

Prein, A.F., Rasmussen, R.M., Ikeda, K., Liu, C., Clark, M.P., Holland, G.J., 2017b. The future intensification of hourly precipitation extremes. Nature Clim. Change 7 (1), 48–52.

Púčik, T., Groenemeijer, P., Rädler, A.T., Tijssen, L., Nikulin, G., Prein, A.F., van Meijgaard, E., Fealy, R., Jacob, D., Teichmann, C., 2017. Future changes in European severe convection environments in a regional climate model ensemble. J. Clim. 30 (17), 6771–6794.

Rasmussen, R., Liu, C., Ikeda, K., Gochis, D., Yates, D., Chen, F., Tewari, M., Barlage, M., Dudhia, J., Yu, W., et al., 2011. High-resolution coupled climate runoff simulations of seasonal snowfall over Colorado: A process study of current and warmer climate. J. Clim. 24 (12), 3015–3048.

Rasmussen, K.L., Prein, A.F., Rasmussen, R.M., Ikeda, K., Liu, C., 2020. Changes in the convective population and thermodynamic environments in convection-permitting regional climate simulations over the United States. Clim. Dynam. 55 (1), 383–408.

Ritter, B., Geleyn, J.-F., 1991. A comprehensive radiation scheme for numerical weather prediction models with potential applications in climate simulations. Am. Meteorol. Soci. 120, 303–325.

Rockel, B., Will, A., Hense, A., 2008. The regional climate model COSMO-CLM (CCLM). Meteorol. Z. 17 (4), 347–348.

Romps, D.M., 2011. Response of tropical precipitation to global warming. J. Atmos. Sci. 68 (1), 123–138.

Romps, D.M., 2016. Clausius–Clapeyron scaling of CAPE from analytical solutions to RCE. J. Atmos. Sci. 73 (9), 3719–3737.

Schär, C., Frei, C., Lüthi, D., Davies, H.C., 1996. Surrogate climate-change scenarios for regional climate models. Geophys. Res. Lett. 23 (6), 669–672.

Schemm, S., Nisi, L., Martinov, A., Leuenberger, D., Martius, O., 2016. On the link between cold fronts and hail in Switzerland. Atmos. Sci. Lett. 17 (5), 315–325. http://dx.doi.org/10.1002/asl.660.

Schulz, J.-P., Vogel, G., Becker, C., Kothe, S., Ahrens, B., 2015. Evaluation of the ground heat flux simulated by a multi-layer land surface scheme using high-quality observations at grass land and bare soil. In: EGU General Assembly Conference Abstracts. In: EGU General Assembly Conference Abstracts, p. 6549, URL https://ui.adsabs.harvard.edu/abs/2015EGUGA..17.6549S.

Seeley, J.T., Romps, D.M., 2015a. The effect of global warming on severe thunderstorms in the united states. J. Clim. 28 (6), 2443–2458.

Seeley, J.T., Romps, D.M., 2015b. Why does tropical convective available potential energy (CAPE) increase with warming? Geophys. Res. Lett. 42 (23), 10–429.

Séférian, R., Nabat, P., Michou, M., Saint-Martin, D., Voldoire, A., Colin, J., Decharme, B., Delire, C., Berthet, S., Chevallier, M., et al., 2019. Evaluation of CNRM earth system model, CNRM-ESM2-1: Role of earth system processes in present-day and future climate. J. Adv. Modelling Earth Syst. 11 (12), 4182–4227.

Seibt, C., Peeters, F., Graf, M., Sprenger, M., Hofmann, H., 2013. Modeling wind waves and wave exposure of nearshore zones in medium-sized lakes. Limnol. Oceanogr. 58 (1), 23–36.

Seifert, A., Beheng, K.D., 2001. A double-moment parameterization for simulating autoconversion, accretion and selfcollection. Atmos. Res. 59–60, 265–281. http://dx.doi.org/10.1016/S0169-8095(01)00126-0.

Seifert, A., Beheng, K., 2006. A two-moment cloud microphysics parameterization for mixed-phase clouds. Part 1: Model description. Meteorol. Atmos. Phys. 92 (1–2), 45–66. http://dx.doi.org/10.1007/s00703-005-0112-4.

Sellar, A.A., Jones, C.G., Mulcahy, J.P., Tang, Y., Yool, A., Wiltshire, A., O'connor, F.M., Stringer, M., Hill, R., Palmieri, J., et al., 2019. UKESM1: Description and evaluation of the UK Earth System Model. J. Adv. Modelling Earth Syst. 11 (12), 4513–4558.

Semazzi, F., 2011. Enhancing Safety of Navigation and Efficient Exploitation of Natural Resources Over Lake Victoria and Its Basin by Strengthening Meteorological Services on the Lake. North Carolina State University Climate Modeling Laboratory Tech. Rep..

Šepić, J., Rabinovich, A.B., 2014. Meteotsunami in the Great Lakes and on the Atlantic coast of the United States generated by the "derecho" of June 29–30, 2012. In: Meteorological Tsunamis: The US East Coast and Other Coastal Regions. Springer, pp. 75–107. http://dx.doi.org/10.1007/978-3-319-12712-5_5.

Shanas, P., Aboobacker, V., Alaa, M.A., Khalid, M.Z., 2017. Superimposed wind-waves in the Red Sea. Ocean Eng. 138, 9–22.

Singh, M.S., Kuang, Z., Maloney, E.D., Hannah, W.M., Wolding, B.O., 2017. Increasing potential for intense tropical and subtropical thunderstorms under global warming. Proc. Natl. Acad. Sci. 114 (44), 11657–11662.

Singleton, A., Toumi, R., 2013. Super-Clausius–Clapeyron scaling of rainfall in a model squall line. Q. J. R. Meteorol. Soc. 139 (671), 334–339.

Sobel, A.H., Camargo, S.J., 2011. Projected future seasonal changes in tropical summer climate. J. Clim. 24 (2), 473–487.

Sobel, A.H., Tippett, M.K., 2018. Extreme events: trends and risk assessment methodologies. In: Resilience. Elsevier, pp. 3–12.

Souverijns, N., Thiery, W., Demuzere, M., Van Lipzig, N.P., 2016. Drivers of future changes in East African precipitation. Environ. Res. Lett. 11 (11), 114011.

Swart, N.C., Cole, J.N., Kharin, V.V., Lazare, M., Scinocca, J.F., Gillett, N.P., Anstey, J., Arora, V., Christian, J.R., Hanna, S., et al., 2019. The Canadian earth system model version 5 (CanESM5. 0.3). Geosci. Model Dev. 12 (11), 4823–4873.

Tatebe, H., Ogura, T., Nitta, T., Komuro, Y., Ogochi, K., Takemura, T., Sudo, K., Sekiguchi, M., Abe, M., Saito, F., et al., 2019. Description and basic evaluation of simulated mean state, internal variability, and climate sensitivity in MIROC6. Geosci. Model Dev. 12 (7), 2727–2765.

Taylor, C.M., Belušić, D., Guichard, F., Parker, D.J., Vischel, T., Bock, O., Harris, P.P., Janicot, S., Klein, C., Panthou, G., 2017. Frequency of extreme sahelian storms tripled since 1982 in satellite observations. Nature 544 (7651), 475–478.

Thiery, W., Davin, E.L., Panitz, H.-J., Demuzere, M., Lhermitte, S., Van Lipzig, N., 2015. The impact of the African Great Lakes on the regional climate. J. Clim. 28 (10), 4061–4085.

Thiery, W., Davin, E.L., Seneviratne, S.I., Bedka, K., Lhermitte, S., Van Lipzig, N.P., 2016. Hazardous thunderstorm intensification over Lake Victoria. Nature Commun. 7 (1), 1–7.

Thiery, W., Gudmundsson, L., Bedka, K., Semazzi, F.H., Lhermitte, S., Willems, P., Van Lipzig, N.P., Seneviratne, S.I., 2017. Early warnings of hazardous thunderstorms over Lake Victoria. Environ. Res. Lett. 12 (7), 074012.

Tiedtke, M., 1989. A comprehensive mass flux scheme for Cumulus parameterization in large-scale models. Am. Meteorol. Soc. 117, 1779–1800.

Torma, C., Giorgi, F., Coppola, E., 2015. Added value of regional climate modeling over areas characterized by complex terrain—Precipitation over the alps. J. Geophys. Res.: Atmos. 120 (9), 3957–3972.

Trapp, R.J., Diffenbaugh, N.S., Brooks, H.E., Baldwin, M.E., Robinson, E.D., Pal, J.S., 2007. Changes in severe thunderstorm environment frequency during the 21st century caused by anthropogenically enhanced global radiative forcing. Proc. Natl. Acad. Sci. 104 (50), 19719–19723.

Trapp, R.J., Hoogewind, K.A., 2016. The realization of extreme tornadic storm events under future anthropogenic climate change. J. Clim. 29 (14), 5251–5265.

Trenberth, K.E., 2011. Changes in precipitation with climate change. Clim. Res. 47 (1–2), 123–138.

Trenberth, K.E., Dai, A., Rasmussen, R.M., Parsons, D.B., 2003. The changing character of precipitation. Bull. Am. Meteorol. Soc. 84 (9), 1205–1218.

Van de Walle, J., Thiery, W., Brousse, O., Souverijns, N., Demuzere, M., van Lipzig, N.P., 2020. A convection-permitting model for the Lake Victoria Basin: evaluation and insight into the mesoscale versus synoptic atmospheric dynamics. Clim. Dynam. 54 (3), 1779–1799. http://dx.doi.org/10.1007/s00382-019-05088-2.

Vanden Broucke, S., Wouters, H., Demuzere, M., van Lipzig, N.P., 2019. The influence of convection-permitting regional climate modeling on future projections of extreme precipitation: dependency on topography and timescale. Clim. Dynam. 52 (9), 5303–5324.

Voldoire, A., Saint-Martin, D., Sénési, S., Decharme, B., Alias, A., Chevallier, M., Colin, J., Guérémy, J.-F., Michou, M., Moine, M.-P., et al., 2019. Evaluation of CMIP6 deck experiments with CNRM-CM6-1. J. Adv. Modelling Earth Syst. 11 (7), 2177–2213.

Volodin, E.M., Mortikov, E.V., Kostrykin, S.V., Galin, V.Y., Lykossov, V.N., Gritsun, A.S., Diansky, N.A., Gusev, A.V., Iakovlev, N.G., Shestakova, A.A., et al., 2018. Simulation of the modern climate using the INM-CM48 climate model. Russian J. Numer. Anal. Math. Modelling 33 (6), 367–374.

Wahle, K., Staneva, J., Koch, W., Fenoglio-Marc, L., Ho-Hagemann, H., Stanev, E.V., 2017. An atmosphere–wave regional coupled model: improving predictions of wave heights and surface winds in the southern North Sea. Ocean Sci. 13 (2), 289–301.

Weisman, M.L., Klemp, J.B., 1982. The dependence of numerically simulated convective storms on vertical wind shear and buoyancy. Mon. Weather Rev. 110 (6), 504–520.

Westra, S., Fowler, H., Evans, J., Alexander, L., Berg, P., Johnson, F., Kendon, E., Lenderink, G., Roberts, N., 2014. Future changes to the intensity and frequency of short-duration extreme rainfall. Rev. Geophys. 52 (3), 522–555.

Woodhams, B.J., Barrett, P.A., Marsham, J.H., Birch, C.E., Bain, C.L., Fletcher, J.K., Hartyley, A.J., Webster, S., Mangeni, S., 2021. Aircraft observations of the lake–land breeze circulation over Lake Victoria. In Review.

Woodhams, B.J., Birch, C.E., Marsham, J.H., Lane, T.P., Bain, C.L., Webster, S., 2019. Identifying key controls on storm formation over the Lake Victoria basin. Mon. Weather Rev. 147 (9), 3365–3390.

Wu, T., Lu, Y., Fang, Y., Xin, X., Li, L., Li, W., Jie, W., Zhang, J., Liu, Y., Zhang, L., et al., 2019. The Beijing climate center climate system model (BCC-csm): The main progress from CMIP5 to CMIP6. Geosci. Model Dev. 12, 1573–1600.

Yoshikane, T., Kimura, F., Kawase, H., Uno, F., 2013. Estimation of the necessary simulation duration for assessing climatic change using the pseudo-global-warming downscaling method in snowy area of Japan. SOLA 9, 157–160. http://dx.doi.org/10.2151/sola.2013-035.

Yukimoto, S., Kawai, H., Koshiro, T., Oshima, N., Yoshida, K., Urakawa, S., Tsujino, H., Deushi, M., Tanaka, T., Hosaka, M., et al., 2019. The Meteorological Research Institute Earth System Model version 2.0, MRI-ESM2. 0: Description and basic evaluation of the physical component. J. Meteorol. Soc. Japan Ser. II.

Zinner, T., Groenemeijer, P., 2012. Thunderstorms: Thermodynamics and organization. In: Atmospheric Physics. Springer, pp. 101–114.

Zscheischler, J., Martius, O., Westra, S., Bevacqua, E., Raymond, C., Horton, R.M., van den Hurk, B., AghaKouchak, A., Jézéquel, A., Mahecha, M.D., Maraun, D., Ramos, A.M., Ridder, N., Thiery, W., Vignotto, E., 2020. A typology of compound weather and climate events. Nat. Rev. Earth Environ. 1, 333–347. http://dx.doi.org/10.1038/s43017-020-0060-z.

Zscheischler, J., Naveau, P., Martius, O., Engelke, S., Raible, C., 2021. Evaluating the dependence structure of compound precipitation and wind speed extremes. Earth Syst. Dyn. 12 (1), 1–16. http://dx.doi.org/10.5194/esd-12-1-2021.

Zscheischler, J., Westra, S., Van Den Hurk, B.J., Seneviratne, S.I., Ward, P.J., Pitman, A., AghaKouchak, A., Bresch, D.N., Leonard, M., Wahl, T., et al., 2018. Future climate risk from compound events. Nature Clim. Change 8 (6), 469–477.